bioRxiv preprint doi: https://doi.org/10.1101/579003; this version posted March 16, 2019. The copyright holder for this preprint (which was not certified by peer review) is the author/funder, who has granted bioRxiv a license to display the preprint in perpetuity. It is made available under aCC-BY 4.0 International license.

Hearing impairment due to *Mir183/96/182* mutations suggests both loss and gain of function effects

Morag A. Lewis*[1,2], Francesca Di Domenico[1], Neil J. Ingham[1,2], Haydn M. Prosser[2], Karen P. Steel[1,2]

[1.] Wolfson Centre for Age-Related Diseases, King's College London, London, SE1 1UL, UK

[2.] Wellcome Trust Sanger Institute, Hinxton, Cambridge, CB10 1SA, UK

* = Corresponding author

Email addresses:

MAL: morag.lewis@kcl.ac.uk

FDD: francesca.di_domenico@kcl.ac.uk

NJI: neil.ingham@kcl.ac.uk

HMP: hmp@sanger.ac.uk

KPS: karen.steel@kcl.ac.uk

bioRxiv preprint doi: https://doi.org/10.1101/579003; this version posted March 16, 2019. The copyright holder for this preprint (which was not certified by peer review) is the author/funder, who has granted bioRxiv a license to display the preprint in perpetuity. It is made available under aCC-BY 4.0 International license.

Abstract

The microRNA miR-96 is important for hearing, as point mutations in humans and mice result in dominant progressive hearing loss. *Mir96* is expressed in sensory cells along with *Mir182* and *Mir183*, but the roles of these closely-linked microRNAs are as yet unknown. Here we describe our physiological, structural and transcriptional analyses of mice carrying null alleles of *Mir182*, and of *Mir183* and *Mir96* together. We found that *Mir183*/*96* heterozygous mice had normal hearing, and although the homozygotes were completely deaf and had severely affected hair cells bundles at four weeks old, the hair cells were still present, unlike mice with a point mutation in *Mir96*. *Mir182* knockout mice showed the mildest effect, developing normal hearing then exhibiting progressive hearing loss. Our transcriptional analyses in both mice reflected these milder phenotypes. We developed a new bioinformatic tool for creating a causal network connecting transcriptional regulators to their misregulated genes using publicly available data (PoPCoRN). Our findings suggest that the gain of novel targets plays an important role in the phenotype caused by a miR-96 mutation.

Keywords: microRNAs, hearing loss, miR-96, networks, miR-183, miR-182

bioRxiv preprint doi: https://doi.org/10.1101/579003; this version posted March 16, 2019. The copyright holder for this preprint (which was not certified by peer review) is the author/funder, who has granted bioRxiv a license to display the preprint in perpetuity. It is made available under aCC-BY 4.0 International license.

Background

The microRNAs miR-96, miR-182 and miR-183 are expressed together on a single transcript in sensory cells, including the retina and the hair cells of the inner ear (Weston et al, 2006; Xu et al, 2007). Point mutations in *Mir96* cause rapidly progressive hearing loss in the diminuendo mouse mutant (*Mir96*^{Dmdo}, (Lewis et al, 2009)) and progressive hearing loss with later onset in human families (Mencia et al, 2009; Solda et al, 2012), and the diminuendo mutation has also been shown to delay maturation of the central auditory system (Schluter et al, 2018). The complete loss of all mature miRNAs from the inner ear results in very early developmental defects including a severely truncated cochlear duct(Friedman et al, 2009; Soukup et al, 2009), while overexpression of the three microRNAs also results in cochlear defects and hearing loss (Weston et al, 2018).

In homozygous *Mir96*^{Dmdo} mice, most of the cochlear hair cells die by 28 days after birth. However, this is not the cause of the hearing loss; even before the onset of normal hearing, homozygote hair cells fail to mature both morphologically and physiologically, remaining in their immature state, and heterozygote hair cells show a developmental delay. miR-96 is thus thought to be responsible for coordinating hair cell maturation (Chen et al, 2014; Kuhn et al, 2011).

MicroRNAs regulate the expression of many other genes by targeting specific sequences in their mRNAs, leading to transcript destabilisation or translational inhibition. Transcriptome analyses of the *Mir96*^{Dmdo} mouse organ of Corti showed that many genes were dysregulated in homozygotes, including several known to be important for hearing which appear to contribute to specific aspects of the diminuendo phenotype (Chen et al, 2014; Kuhn et al, 2011; Lewis et al, 2016; Lewis et al, 2009). However, the diminuendo mutation is a single base pair change in the seed region of the microRNA which is critical for correct targeting, and it is not clear to what extent the diminuendo mutant phenotype is the result of the loss of normal targets of miR-96, and how much is due to the gain of novel targets.

Here we present data from mice carrying a knockout allele of *Mir182*, and mice carrying a double knockout allele of *Mir183* and *Mir96* (*Mir183/96*), generated through a mouse miRNA knockout program (Prosser et al, 2011). We carried out Auditory Brainstem Response (ABR) and Distortion Product Otoacoustic Emission (DPOAE) tests to characterise their hearing, scanning electron and confocal microscopy to examine their hair cells and synapses, and mRNA sequencing (RNA-seq) to study their transcriptomes. We have also developed a computational tool for connecting regulators with misregulated genes, in order to explore the regulatory networks controlled by miR-96, miR-182 and miR-183. While both mouse mutants do exhibit hearing loss, their electrophysiological and transcriptional phenotypes differ from the diminuendo mouse, offering insight into the function of these regulators which are so important for hair cell development and function.

Results

Mir183/96 and *Mir182* knockout mice

Two mouse lines were used in this study; a knockout of *Mir182* (*Mir182*$^{tm1Hmpr/Wtsi}$, referred to from here on as *Mir182*^{ko}) and a knockout of both *Mir183* and *Mir96* (*Mirc40*$^{tm1Hmpr/WtsiOulu}$, referred to from here on as *Mir183/96*^{dko}), which are only 116bp apart, making it technically challenging to generate two separate knockouts. The mice were generated and maintained on the C57BL/6N

bioRxiv preprint doi: https://doi.org/10.1101/579003; this version posted March 16, 2019. The copyright holder for this preprint (which was not certified by peer review) is the author/funder, who has granted bioRxiv a license to display the preprint in perpetuity. It is made available under aCC-BY 4.0 International license.

genetic background. C57BL/6 mice are known to have age-related hearing loss, partly due to the *Cdh23*^{ahl} allele (Noben-Trauth et al, 2003). Higher frequencies are affected first, after four weeks of age, while the lower frequencies remain unaffected up to 6 months old (Li & Borg, 1991). We observed a similar pattern in wildtype mice from both the *Mir183/96*^{dko} and *Mir182*^{ko} lines, which exhibited mild progressive hearing loss at 24-42kHz from 8 weeks old but retained good hearing sensitivity at frequencies between 3-12kHz up to six months old (Fig 1).

For the *Mir183/96*^{dko} mice, 43 out of 242 mice (17.8%) from heterozygote by heterozygote matings were homozygous for the *Mir183/96* null allele, which is lower than the expected production (25%), suggesting that the absence of *Mir96* and/or *Mir183* has a small impact on viability (p=0.029, chi-squared test). For the *Mir182*^{ko} mice, 42 homozygotes out of 152 pups in total (27.6%) were produced from heterozygote by heterozygote matings, which is consistent with the mutation having no impact on viability.

miRNA expression

We carried out qPCR to test the expression levels of the three microRNAs in the organs of Corti of wildtypes, heterozygotes and homozygotes of each knockout. In *Mir183/96*^{dko} homozygotes, there was no detectable expression of *Mir183* or *Mir96*. Likewise, in *Mir182*^{ko} homozygotes there was no detectable expression of *Mir182* (Appendix Figure S1). The levels of expression in heterozygotes of both knockouts was variable, as was the expression of *Mir182* in *Mir183/96*^{dko} homozygotes, and *Mir183* and *Mir96* in *Mir182*^{ko} homozygotes. It is likely that this is because we lack a proper microRNA control for sensory tissue in the inner ear. We used *Mir99a*, which is expressed in almost all cell types in the cochlea, including hair and supporting cells (Friedman et al, 2009), but because *Mir183*, *Mir182* and *Mir96* are also expressed in hair cells, it is possible that the mutant alleles affect the expression of *Mir99a* in hair cells, making it an unreliable calibrator between wildtype, heterozygote and homozygote. A better calibrator would be a microRNA expressed only in supporting cells and not in hair cells.

Auditory brainstem response (ABR), distortion product otoacoustic emissions (DPOAEs) and waveform analysis

Mir183/96^{dko} homozygous mice were profoundly deaf, with most showing no response at the highest sound level tested (95dB SPL) at any of the ages tested (14 days to six months old). In contrast, *Mir182*^{ko} homozygotes exhibited only a mild hearing loss starting at higher frequences and progressing with age to lower frequencies (Fig 1). The ABR thresholds of *Mir183/96*^{dko} and *Mir182*^{ko} heterozygotes were similar to the wildtypes at all ages (Fig 1, see Appendix Figures S2, S3 for individually plotted traces). We examined ABR waveforms for the 12kHz stimulus (the most sensitive frequency) but found no differences between waveforms of *Mir183/96*^{dko} heterozygotes and wildtypes, or between *Mir182*^{ko} homozygotes and wildtypes (Appendix Figure S4). *Mir182*^{ko} mutant mice showed no sign of a vestibular defect (circling, head-bobbing or hyperactivity) up to six months old. However, *Mir183/96*^{dko} homozygotes did show increasing incidence of hyperactivity with age (Appendix Figure S5). We measured DPOAEs at 8 weeks old, and found no difference in the responses or thresholds between wildtype and heterozygous *Mir183/96*^{dko} mice, while homozygotes had severely abnormal responses (Appendix Figure S6). *Mir182*^{ko} homozygotes had raised DPOAE thresholds at high frequencies compared to wildtypes (Appendix Figure S6), which matched the difference in their ABR thresholds at 8 weeks (Fig 1).

bioRxiv preprint doi: https://doi.org/10.1101/579003; this version posted March 16, 2019. The copyright holder for this preprint (which was not certified by peer review) is the author/funder, who has granted bioRxiv a license to display the preprint in perpetuity. It is made available under aCC-BY 4.0 International license.

Noise exposure

As heterozygous *Mir183/96*^{dko} mice showed no auditory deficit, in contrast to the hearing loss seen in diminuendo heterozygotes and in humans carrying one mutant *MIR96* allele, we asked if these heterozygous mice might be more sensitive to noise-induced damage. One day after noise exposure (2 hours of 8-16kHz octave-band noise at 96dB SPL) at 8 weeks old, both *Mir183/96*^{dko} heterozygous and wildtype mice showed a marked increase in thresholds at 12kHz and above compared to unexposed control littermates (Fig 2). Three days after noise exposure the 12kHz thresholds had recovered, but there was still a noticeable elevation at higher frequencies. By 7 days after exposure, all thresholds had recovered completely; there was no difference between exposed and unexposed mice, wildtypes or heterozygotes (Fig 2). We measured the amplitude of wave 1 of the ABR waveform to look for a reduced neural response, which has been reported in CBA/CaJ mice after noise exposure (Kujawa & Liberman, 2009) and is thought to be due to neuronal loss in the cochlea. No difference was observed in the amplitude of wave 1 at 12kHz (Fig 2). At 24kHz, we observed a much greater effect, such that in most animals wave 1 was too poorly defined to measure the amplitude one day after exposure. However, both wildtype and heterozygote wave 1 amplitudes had recovered by 28 days after exposure, and did not look any different to mice which had not been exposed (Fig 2; Appendix Figure S7).

Since there was a significant difference in the higher frequencies between the unexposed heterozygotes and wildtypes at 8 weeks old (Fig 2), but we did not see any difference in our original ABR tests (Fig 1), we compared the ABR thresholds from all mice tested at 8 weeks old (Appendix Figure S8). At high frequencies (30-42kHz) the thresholds were very variable in both heterozygotes and wildtypes. The differences in the means at 36kHz and 42kHz are statistically significant (P = 0.001, P=0.000; mixed linear model pairwise comparison), but given the variability we suggest that this is not biologically relevant.

Hair cells and innervation

We examined the organ of Corti using scanning electron microscopy, and found that hair cells in homozygous *Mir183/96*^{dko} mice were severely affected at four weeks old (Fig 3), with many hair bundles missing entirely. Where present, the stereocilia bundles of both outer and inner hair cells show splaying and fusion, and the “staircase” arrangement of stereocilia rows is disrupted. The inner hair cells of *Mir183/96*^{dko} heterozygotes are unaffected, but the outer hair cells’ upper surface appear slightly smaller and rounder in shape than the wildtype outer hair cells (Fig 3). Their stereocilia bundles also appear smaller and more rounded than normal, with more pronounced tapering in height and overlap of shorter stereocilia rows with taller rows towards the two ends of each bundle.

Both outer and inner hair cells of four week old *Mir182*^{ko} heterozygotes and homozygotes resembled wildtype hair cells at the 12kHz and 24kHz regions (Fig EV1), corresponding to their normal ABR thresholds at that age. At eight weeks old, when hearing loss is evident at 24kHz and higher (Fig 1), we also saw no systematic differences in the appearance of the organ of Corti between wildtype, heterozygote and homozygote (Fig 4).

We examined the distribution of unmyelinated neurons using anti-neurofilament labelling in whole-mount organ of Corti preparations, but there appeared to be no systematic differences in either

bioRxiv preprint doi: https://doi.org/10.1101/579003; this version posted March 16, 2019. The copyright holder for this preprint (which was not certified by peer review) is the author/funder, who has granted bioRxiv a license to display the preprint in perpetuity. It is made available under aCC-BY 4.0 International license.

mutant compared with littermate controls (Fig EV2). We also examined synapses using anti-Ribeye antibody to mark presynaptic ribbons and anti-GluR2 to mark postsynaptic densities, and found a significant reduction in the number of colocalised pre- and postsynaptic markers in *Mir183/96*^{dko} homozygotes (Fig 5, p=0.036, Wilcoxon rank sum test). No difference in synapse counts was observed in *Mir182*^{ko} homozygotes.

Transcriptome analysis

To investigate the impact of the *Mir182*^{ko} and *Mir183/96*^{dko} mutations on gene expression we carried out RNAseq of isolated organ of Corti preparations from postnatal day (P)4 homozygotes and sex-matched littermate wildtype controls. This age was chosen based on our previous work in *Mir96*^{Dmdo} mice, because hair cells were still present at P4 in *Mir96*^{Dmdo} homozygotes (Lewis et al, 2009). By analysis of the RNA-seq data, thirty-four genes were identified as significantly (FDR < 0.05) misregulated in *Mir183/96*^{dko} homozygotes, 22 upregulated and 12 downregulated compared with wildtype littermates. Many of the upregulated genes have sequences complementary to either the miR-96 seed region or the miR-183 seed region in their 3'UTRs (Table EV1). Of this list of 34 genes, *Hspa2*, *Ocm, Myo3a*, *Slc26a5* and *Sema3e* were also all found to be misregulated in the microarrays carried out on *Mir96*^{Dmdo} mice at P4 and/or P0 (Lewis et al, 2016; Lewis et al, 2009), and in each case the misregulation is in the same direction (Table EV1). The most upregulated gene was *Gm904* (log fold change (FC)=2.33), and the most downregulated gene was *Gm29100* (logFC=-6.17), which is a greater range than that observed in the *Mir96*^{Dmdo} data, where the most upregulated gene was *1110017D15Rik* (logFC=2.01) and the most downregulated gene was *Ocm* (logFC=-3.99). Genes were chosen for confirmatory testing by qPCR from P4 organ of Corti preparations based on their expression in hair cells compared to non-sensory cells as reported in the gEAR portal (http://www.umgear.org), which displays data from the mouse organ of Corti at various ages; we used P0 data(Cai et al, 2015; Elkon et al, 2015). We tested 19 genes and all but three were confirmed correct (Table EV1, Fig EV3); those that were not confirmed by qPCR were either not misregulated or failed the significance test, and no genes were significantly misregulated in the opposite direction. Of the genes misregulated in *Mir183/96*^{dko} homozygotes, five are known deafness genes; *Myo3a*, *Slc26a5* and *Tmc1* underlie deafness in mice and humans (Kurima et al, 2002; Liberman et al, 2002; Liu et al, 2003; Vreugde et al, 2002; Walsh et al, 2002; Walsh et al, 2011), while mutations in *Sema3e* cause deafness in people (Lalani et al, 2004), and mice homozygous for a mutant allele of *Ocm* exhibit progressive hearing loss (Tong et al, 2016).

Three genes were found to be significantly (FDR < 0.05) upregulated in the *Mir182*^{ko} homozygotes by RNA-seq, one of which, *Ppm1l*, has sequences complementary to the seed region of miR-182 (Table EV1). The other two, *Grp* and *Ccer2*, were also upregulated in the *Mir183/96*^{dko} homozygotes. No genes were significantly downregulated. We tested these genes by qPCR, and also tested *Slc26a5* and *Ocm* (which were strongly downregulated in *Mir96*^{Dmdo} homozygotes (Lewis et al, 2009)), and found that only the upregulation of *Grp* was confirmed. *Ccer2* and *Ppm1l* were upregulated but not significantly, and *Slc26a5* and *Ocm* were downregulated but again, not significantly (Table EV1, Fig EV3).

To assess the impact of these miRNA knockouts on a genome-wide level, we used Sylamer (van Dongen et al, 2008) to measure the enrichment and depletion of heptamers in the 3'UTRs of each gene list, ranked from most upregulated to most downregulated. In the *Mir183/96*^{dko} gene list, the

bioRxiv preprint doi: https://doi.org/10.1101/579003; this version posted March 16, 2019. The copyright holder for this preprint (which was not certified by peer review) is the author/funder, who has granted bioRxiv a license to display the preprint in perpetuity. It is made available under aCC-BY 4.0 International license.

sequence complementary to the seed region of miR-96 was markedly enriched in the upregulated genes (red line, figure 6A), and the sequence complementary to the seed region of miR-183 has a small peak towards the centre of the graph (dark blue line, figure 6A). There were no miRNA seed region heptamers enriched in the *Mir182*^{ko} gene list (figure 6B), but the TATTTAT heptamer which is enriched in the *Mir182*^{ko} downregulated genes (yellow line, figure 6B) resembles a portion of an AU-rich element. These are 50-150bp sequence elements found in 3'UTRs, and are typically involved in mRNA destabilising via a deadenylation-dependent mechanism (reviewed in (Barreau et al, 2005; Chen & Shyu, 1995)). AU-rich elements, and TATTTAT in particular, are enriched in 3'UTR regions which have multiple RNA-binding protein binding sites, and it has been suggested that RNA-binding proteins compete with the RISC complex to bind to miRNA target sites within these regions (Plass et al, 2017). It is possible that this TATTTAT signal, which is enriched in the genes downregulated in *Mir182*^{ko} homozygote hair cells, is the result of a change in the binding of RNA-binding proteins in the absence of miR-182.

Differential splicing

Splicing patterns can be affected by a microRNA if it targets a splicing factor, as has been shown for miR-133a and nPTB (Boutz et al, 2007), so we analysed the *Mir183/96*^{dko} and *Mir182*^{ko} RNA-seq data for evidence of alternative splicing events. Tools which test RNA-seq data for differential splicing of mRNAs are not as well established as those for measuring differential expression, and there is great variability in the results depending on which method is used(Liu et al, 2014). We therefore used three different tools to test for differential splicing, which all take a different approach. Cuffdiff (from the Cufflinks package(Trapnell et al, 2010)) maps reads to individual transcripts in order to estimate the relative abundance of each isoform. This can introduce uncertainty in the case of reads which map to exonic regions shared by more than one transcript. JunctionSeq(Hartley & Mullikin, 2016), is a count-based tool which tests read counts belonging to exonic regions specific to individual transcripts, avoiding the problem of shared regions but potentially missing isoforms which have no unique exons. Leafcutter, a very recently developed algorithm, tests for differential splicing by using reads which span exon-exon junctions, in effect focussing on the excised intron(Li et al, 2016).

All three tools detected significant differential splicing in *Mir183/96*^{dko} homozygotes compared to their wildtype littermates (Appendix Table S1), but only three genes were identified by more than one tool; *Ppp3cb* and *Zfp618* (by Leafcutter and JunctionSeq), and *Il17re* (by Leafcutter and Cuffdiff). One of the advantages of Leafcutter and JunctionSeq is that they identify the sites at which they detect differential splicing occurring, which allowed us to test their results. We designed primers to cover the junctions and/or exons which were highly differentially spliced (15 genes; appendix Table S2) and sequenced PCR reactions from cDNA made from organ of Corti RNA from *Mir183/96*^{dko} homozygotes and wildtypes. We found no evidence of the differential splicing detected by either tool, but evidence of a novel isoform of *Stard9* was detected by JunctionSeq. The novel isoform includes an exon (ENSMUSE00001437951) previously assigned to a transcript subject to nonsense-mediated decay (transcript ENSMUST00000140843), but the exons following ENSMUSE00001437951 in our results belong to the protein-coding transcript (ENSMUST00000180041). Exon ENSMUSE00001437951 is 72bp long, so does not introduce a frameshift, and its inclusion may result in a functional *Stard9* protein with 24 extra amino acids. The novel splicing was present in both wildtype and homozygous *Mir183/96*^{dko} RNA (Appendix Figure S9).

bioRxiv preprint doi: https://doi.org/10.1101/579003; this version posted March 16, 2019. The copyright holder for this preprint (which was not certified by peer review) is the author/funder, who has granted bioRxiv a license to display the preprint in perpetuity. It is made available under aCC-BY 4.0 International license.

JunctionSeq did not predict any significant differential splicing in *Mir182*^{ko} homozygotes. Leafcutter and Cuffdiff identified some genes with differential splicing (Appendix Table S1), but there were no genes common to both predictors. Two genes, *Ube4a* and *Nrxn1*, were predicted to have alternative splicing present in the homozygote and not in the wildtype, but when we sequenced their mRNA from *Mir182*^{ko} homozygotes and wildtypes, we found no differences in the splicing pattern.

Immunohistochemistry

We carried out antibody stains on sections from the inner ear at P4, to check for the presence of Ocm (oncomodulin) and Slc26a5 (prestin) protein in the hair cells. Ocm staining is faint at P4, stronger in the basal turn of the cochlea, but prestin staining is clearly visible at that stage. We observed prestin staining in *Mir183/96*^{dko} homozygotes, but no stain for Ocm, while both proteins were present in the wildtype littermate controls (Appendix Figure S10). Although immunohistochemistry is not a quantitative technique, this correlates with the qPCR results, which showed that *Ocm* RNA was nearly absent in *Mir183/96*^{dko} homozygotes, while *Slc26a5* RNA levels were about 30% of wildtype levels (Fig EV3). Ocm and Prestin staining was visible in *Mir182*^{ko} homozygotes and their wildtype littermate controls (Appendix Figure S10).

Network analysis

We took two approaches to network analysis. First, we used Ingenuity Pathway Analysis to construct putative causal networks using the misregulated genes in each dataset with FDR<0.05, as follows. Upstream regulators which could explain the observed misregulation were identified through the Ingenuity Knowledge Base, a manually curated set of observations from the literature and from third-party databases. The activation or inhibition of each upstream regulator was calculated based on the observed misregulation of its target genes. Causal networks were then constructed to link the upstream regulators through a “root” regulator further upstream, again using the Ingenuity Knowledge Base (described in detail in (Kramer et al, 2014)). The resulting networks were filtered based on their activation z-score, which is a measure of the match of observed and predicted misregulation patterns. The z-score is not just a measure of significance but also a prediction of the activation of the upstream root regulator (Kramer et al, 2014); scores below -2 are classed as significant by Ingenuity Pathway Analysis and indicate predicted downregulation or reduced activation of the root regulator, while scores above 2 are also considered significant and indicate predicted upregulation or increased activation of the root regulator. For the *Mir183/96*^{dko} homozygotes, only four upstream regulators were given a z-score < -2, three more had z-scores < -1.7 and one had a z-score > 1.7. These eight upstream regulators, Bdnf, Cshl1, H2afx, Kcna3, Kit, Myocd, Prkaca and Pth, explain between them the misregulation of 14 genes (Fig 7). There were too few genes significantly misregulated in the *Mir182*^{ko} RNA-seq data to obtain any causal networks with a significant activation z-score, but Ret and Adcyap1 were identified as immediate upstream regulators of Grp.

The PoPCoRN tool

The IPA networks did not connect the misregulated genes to any of the three microRNAs, probably because each microRNA controls a regulatory cascade, and the IPA causal networks have a maximum depth of 3, which may not be enough to reach the level of direct targets. We therefore developed the PoPCoRN (prediction of potential causal regulatory networks) tool to make use of

bioRxiv preprint doi: https://doi.org/10.1101/579003; this version posted March 16, 2019. The copyright holder for this preprint (which was not certified by peer review) is the author/funder, who has granted bioRxiv a license to display the preprint in perpetuity. It is made available under aCC-BY 4.0 International license.

publicly available regulatory data to connect misregulated genes to a known top-level regulator, and used this to analyse the *Mir183/96*^{dko} and *Mir182*^{ko} datasets. PoPCoRN requires a list of misregulated genes and a list of genes at which to stop, the upstream regulators beyond which no connections will be explored. We used the significantly misregulated genes (FDR < 0.05) from each RNA-seq experiment (Table EV1) and used the relevant microRNAs as the genes at which to stop. The PoPCoRN tool is freely available from github (https://github.com/moraglewis/PoPCoRN).

The resulting *Mir183/96*^{dko} network consists of 100 genes and 325 links. Twenty seven misregulated genes have been included, 13 of them predicted targets of either miR-183 or miR-96 or both. Five misregulated genes were left out completely due to having no known regulatory links in our compiled potential links (*Ccer2*, *Gm904*, *Myo3a*, *Rn7s1* and *P2rx3*) (Fig 8A). We carried out a network analysis using the Cytoscape Network Analyser tool to calculate the degree and betweenness centrality of each node (gene). A node's degree is the number of edges connecting it to other nodes, and its betweenness centrality measures how important it is for connecting distant parts of the network. The node with the highest degree is *Trp53*, with 23 edges. Most nodes have 9 or fewer edges (Fig 8A), but 21 have 10 or more edges (listed in Table 1). Among them are *Trp53*, *Sp1*, *Tgfb1*, *Tnf* and *Fos*, which were also genes of interest in the manually-created network based on the *Mir96*^{Dmdo} microarray data (Lewis et al, 2016). Of these 21 nodes with 10 or more edges, only *Trp53* also has a high betweenness centrality, and none are known to be misregulated in *Mir183/96*^{dko} homozygotes.

We also carried out the same analysis using the microarray and qRTPCR data from *Mir96*^{Dmdo} (Lewis et al, 2016) (133 input genes with adjusted P < 0.05). The resulting network has 231 genes and 869 links, and includes 74 of the 133 misregulated genes (Fig 8B), in contrast to the network created manually in our previous work, which consisted of 103 genes with 343 links, and included only 57 of the misregulated genes (Lewis et al, 2016). In this new *Mir96*^{Dmdo} network, the node with the highest degree is *Chrna9*, with 52 edges. There are 16 nodes with 20 or more edges (Appendix Figure S11), several of which have a high betweenness score (*E2f2*, *Trp53*, *Ccnd1*, *Nfkb1*, and *Tgfb1*), indicating they are important for connecting the network. Of these genes, *Trp53*, *Cdkn1a*, *Ccnd1*, *Tcf7*, *Tnf*, *Cited1*, *E2f2*, *Kit*, *Sp1*, *Nfkb1*, *Tgfb1* and *Zfp36* are shared between the *Mir183/96*^{dko} network and the *Mir96*^{Dmdo} network.

Table 1. Nodes with high edge count in the *Mir183/96*^{dko} network (A) and the *Mir96*^{Dmdo} network (B).

A. *Mir183/96*^{dko} network			**B. *Mir96*^{Dmdo} network**		
Name	**Betweenness Centrality**	**Edge count**	**Name**	**Betweenness Centrality**	**Edge count**
Trp53	0.13746053	23	Chrna9	0.0362401	52
Cdkn1a	0.03539795	20	E2f2	0.08964053	35
Jun	0.0504376	19	Kit	0.01824851	32
Kit	0.07009055	19	Trp53	0.06524623	31
Ccnd1	0.03140771	18	Tcf7	0.00466947	29
Sp1	0.06430619	17	Ccnd1	0.06170119	28
E2f2	0.07545511	17	Nfkb1	0.07381624	27
Nfkb1	0.05583079	14	Cdkn1a	0.04701467	27
Bmyc	0.08356977	14	Cited1	0.03174124	27

bioRxiv preprint doi: https://doi.org/10.1101/579003; this version posted March 16, 2019. The copyright holder for this preprint (which was not certified by peer review) is the author/funder, who has granted bioRxiv a license to display the preprint in perpetuity. It is made available under aCC-BY 4.0 International license.

Tgfb1	0.03107345	13	Tnf	0.13261219	26
Tcf7	0.03438013	13	Esr2	0.02072591	25
Ifng	0.01355005	12	Tgfb1	0.06949546	24
Ar	0.02784885	12	Ezh2	0.03207739	24
Zfp36	0.05360802	12	Zfp36	0.05464577	23
Cited1	0.0177209	12	Sp1	0.04077559	21
Pex5	0.00364178	12	Rest	0.03264786	20
Mir96	0	11			
Fos	0.07432304	11			
Hnf4a	0.07077422	11			
Tnf	0.07227286	10			
Stat3	0.03661371	10			

There are six genes which were found to be significantly misregulated in both the *Mir183/96*^{dko} homozygote RNAseq data and the *Mir96*^{Dmdo} homozygote microarray data; *Hspa2*, *Ocm*, *Slc26a5*, *Sema3e*, *St8sia3* and *Myo3a*. We used the misregulation values from the *Mir183/96*^{dko} RNA-seq data to connect just these six genes with miR-96. As before, *Myo3a* could not be linked in due to having no known regulators, and *St8sia3* and *Hspa2* are themselves predicted to be direct targets of miR-96, but the other three were connected through two miR-96 targets; Zic2 and Nr3c1 (Fig 8C).

It is possible that the difference between the transcriptomes of *Mir183/96*^{dko} knockout mice and *Mir96*^{Dmdo} mice is due to the different backgrounds. We looked for differences in predicted targets in the 3'UTRs of the C57BL/6NJ and C3H/HeJ genome sequences (Adams et al, 2015), which were the closest genome sequences to our mutant backgrounds available, and found that 1585 genes had the same number of seed matches, and 13 genes had seed matches in both strains, but not the same number of matches. 36 genes had no seed matches in the C57BL/6NJ sequence but had one or more match in the C3H/HeJ sequence, and 47 genes had no seed matches in the C3H/HeJ sequence, but one or more in the C57BL/6NJ sequence (Appendix Table S3). None of these 83 genes, nor the 52 with no sequence available in one or the other strain, were in the list of miR-96 targets used for network creation.

The *Mir182*^{ko} network is very small, being based on three input genes: *Ppm1l*, *Ccer2* and *Grp*. *Ccer2* could not be included, due to the lack of any known regulators, and *Ppm1l* is a predicted target of miR-182. *Grp* is linked to miR-182 through three other genes, *Foxo3*, *Trp53* and *Hnf4a* (Fig 8D).

bioRxiv preprint doi: https://doi.org/10.1101/579003; this version posted March 16, 2019. The copyright holder for this preprint (which was not certified by peer review) is the author/funder, who has granted bioRxiv a license to display the preprint in perpetuity. It is made available under aCC-BY 4.0 International license.

Discussion

Comparison of the auditory and vestibular phenotypes of *Mir183/96*^{dko} knockout mice and *Mir96*^{Dmdo} mice

Mice heterozygous for the *Mir96*^{Dmdo} point mutation exhibit early-onset rapid progressive hearing loss; even at P15 they have very raised thresholds (Kuhn et al, 2011). We initially concluded that this was more likely to be due to haploinsufficiency than to the gain of novel targets, because humans heterozygous for different point mutations also had progressive hearing loss (Mencia et al, 2009). However, heterozygous *Mir183/96*^{dko} mice have ABR thresholds and DPOAE responses resembling the wildtype, and there is no difference in thresholds or wave 1 amplitudes of heterozygotes after noise exposure. Two recent studies of different knockout alleles targeting the entire microRNA cluster (miR-183/96/182) found that heterozygotes also exhibited normal hearing (Fan et al, 2017; Geng et al, 2018). It is possible that the more severe phenotype seen in *Mir96*^{Dmdo} heterozygotes is due to the acquisition of new targets by the mutant microRNA, or it could be an effect of the different background as the *Mir96*^{Dmdo} allele was generated by ENU mutagenesis on a C3HeB/FeJ background in contrast to the C57BL/6N background of the *Mir183/96*^{dko} allele or the reported knockouts of the entire cluster, which were created in 129S2 (Lumayag et al, 2013) or 129SV6 (Fan et al, 2017) ES cells which were then injected into C57BL/6J blastocysts and crossed onto the C57BL/6J background (Fan et al, 2017; Lumayag et al, 2013). Mice homozygous for the *Mir183/96*^{dko} allele showed no auditory brainstem responses at all ages tested from 14 days old onwards, and in this they resemble the *Mir96*^{Dmdo} homozygotes, where the compound action potentials recorded from the round window of the cochlea were undetectable at four weeks old (Lewis et al, 2009).

The vestibular phenotype is also different; *Mir96*^{Dmdo} homozygotes circle by three weeks old, whereas a milder phenotype of variable hyperactivity was observed only in some *Mir183/96*^{dko} homozygotes, the prevalence increasing with age (Appendix Figure S5). Circling is a more severe manifestation of vestibular dysfunction than hyperactivity. This could again be due to the C3HeB/FeJ background, because *Mir96*^{Dmdo} mice carry the *Pde6b*^{rd1} mutation causing retinal degeneration (Pittler & Baehr, 1991) and are blind by adulthood. The *Mir183/96*^{dko} allele was generated on a C57BL/6N background, and the mice can see, which may partially compensate for the lack of vestibular sensory input, reducing the severity of the observed phenotype. It is notable that mice lacking the entire miR-183/96/182 cluster (on a mixed background of C57BL/6J and either 129S2 or 129SV6) exhibit both persistent circling behaviour and retinal defects (Fan et al, 2017; Lumayag et al, 2013).

Stereocilia bundles and innervation in *Mir183/96*^{dko} mice and *Mir96*^{Dmdo} mice

The hair cells of *Mir96*^{Dmdo} homozygous mice are present at four days old but appear abnormal, and by 28 days old have degenerated completely (Lewis et al, 2009). In *Mir183/96*^{dko} homozygotes, however, some hair cell bundles are still visible at P28, although they are severely disorganised (Fig 3). In *Mir183/96*^{dko} heterozygotes, IHCs are normal and the OHC stereocilia bundles appear to be slightly misshapen (Fig 3), but this is not reflected in their ABR thresholds or DPOAE responses, which are normal (Fig 1 and Fig S5). *Mir96*^{Dmdo} heterozygotes, which are deaf by P28, have a more severe phenotype, with fused stereocilia and hair cell degeneration as well as misshapen stereocilia bundles in outer hair cells, and smaller stereocilia bundles in inner hair cells (Lewis et al, 2009).

bioRxiv preprint doi: https://doi.org/10.1101/579003; this version posted March 16, 2019. The copyright holder for this preprint (which was not certified by peer review) is the author/funder, who has granted bioRxiv a license to display the preprint in perpetuity. It is made available under aCC-BY 4.0 International license.

Mir96^{Dmdo} homozygotes exhibit disorganised innervation (Kuhn et al, 2011), but the innervation of *Mir183/96*^{dko} homozygotes looked no different to wildtype or heterozygous mice at P28 (Fig EV2), although we found significantly fewer colocalised pre- and postsynaptic densities on the homozygote inner hair cells (Fig 5). Heterozygote *Mir183/96*^{dko} mice showed no differences in innervation or synapse counts (Fig EV2, Fig 5). Similar to the physiological phenotype, the structural phenotype of *Mir183/96*^{dko} heterozygotes is much less severe than that of *Mir96*^{Dmdo} heterozygotes.

Transcriptome data from *Mir183/96*^{dko} mice suggest that the gain of novel targets plays an important role in the phenotype resulting from point mutations in *Mir96*.

We originally hypothesised that the major effect of the *Mir96*^{Dmdo} mutation on hearing was most likely mediated by a reduced level of downregulation of the normal target mRNAs (Lewis et al, 2009), because two different point mutations in the human *MIR96* seed region also led to hearing loss but each mutation is predicted to have different novel targets than the other seed region point mutations. However, the difference in the transcriptomes, along with the normal ABR thresholds of *Mir183/96*^{dko} heterozygotes, suggest that the gain of novel target mRNAs is also important for the diminuendo phenotype. The *Mir183/96*^{dko} transcriptome bears some resemblance to that of the *Mir96*^{Dmdo} transcriptome from our previous studies (Lewis et al, 2016; Lewis et al, 2009), but, as with the physiological and structural phenotypes, the effect of missing both miR-183 and miR-96 appears to be milder than the effect of a point mutation in the miR-96 seed region. Only 34 genes were identified as significantly misregulated by RNA-seq in the current study of *Mir183/96*^{dko}, compared to 86 genes found to be significantly misregulated in the *Mir96*^{Dmdo} P4 microarray (Lewis et al, 2009) , and only six genes are similarly misregulated in both datasets (including the *Mir96*^{Dmdo} P0 microarray); *Hspa2*, *Ocm, Myo3a*, *Slc26a5*, *St8sia3* and *Sema3e* (Table EV1). Some of the differences will be due to certain genes not being present on the microarray assay when it was carried out, such as *Ccer2*, and some may be the result of the different genetic background. We aimed to minimise this by use of the sex-matched wildtype littermates as controls, but it isn't possible to entirely eliminate the effect of genetic background; there are 83 genes which lack miR-96 seed region matches in one background compared to the other (Appendix Table S3), and any of those may be contributing to the phenotype. Much of the difference, however, is likely to be due to the loss of miR-183 in the *Mir183/96*^{dko} homozygotes and the presence of the mutant miR-96 in *Mir96*^{Dmdo} homozygotes. We were unable to confirm any of the predicted differential mRNA splicing in *Mir183/96*^{dko} and *Mir182*^{ko} homozygotes, suggesting that differential splicing is unlikely to play a large part in the mutant phenotypes.

Combining network analyses from *Mir183/96*^{dko} and *Mir96*^{Dmdo} transcriptomes suggests potential intermediate genes which mediate regulation by miR-96.

Our network analyses suggest multiple regulators which could be responsible for mediating the effect of miR-96 on the transcriptome. The network created using five of the six genes misregulated in both the *Mir183/96*^{dko} and *Mir96*^{Dmdo} transcriptome datasets implicates *Zic2* and *Nr3c1* as important targets for miR-96 (Fig 8). Zic2 is a zinc finger transcription factor which is required for normal inner ear development and *Zic2* mutant mice exhibit gross malformations in cochlear and vestibular morphology (Chervenak et al, 2014). The *Nr3c1* gene encodes the glucocorticoid receptor GR, which is also known to be expressed in the inner ear (Erichsen et al, 1998; ten Cate et al, 1993), but no hearing or vestibular phenotypes have been reported on the Mouse Genome Informatics

bioRxiv preprint doi: https://doi.org/10.1101/579003; this version posted March 16, 2019. The copyright holder for this preprint (which was not certified by peer review) is the author/funder, who has granted bioRxiv a license to display the preprint in perpetuity. It is made available under aCC-BY 4.0 International license.

resource (http://www.informatics.jax.org) (Smith et al, 2018) for mice carrying mutations in the gene. Both *Zic2* and *Nr3c1* genes are expressed very strongly in nonsensory cells of the organ of Corti at P0, with little to no expression in the hair cells, which fits with the evidence that they are targets of a microRNA expressed in hair cells (expression was visualised in the gEAR portal (http://www.umgear.org), data from (Cai et al, 2015), which compared *Atoh1*-expressing cells to non-*Atoh1*-expressing cells at P0. The non-sensory cell to hair cell expression ratio for *Nr3c1* is 7.69, while for *Zic2* it is 23.48, and for *Hprt*, a housekeeping gene, it is 0.68).

The role of *Mir183* in hearing remains unclear

The lack of a *Mir183*-specific mutation means that the effect of miR-183 alone is difficult to ascertain from our data. The relatively low mid-range peak for the miR-183 seed region in our Sylamer analysis of the RNA-seq data (Fig 6) implies that the lack of miR-183 has less of a global effect on the transcriptome than the lack of miR-96, and the network analysis reflects this; apart from its predicted targets, there are no downstream genes whose misregulation can be attributed to miR-183 alone (Fig 8A). In the network generated from the *Mir183/96* data, the only miR-183 targets which regulate downstream genes are also miR-96 targets.

Mice lacking *Mir182* display a mild hearing loss phenotype with no obvious changes in stereocilia bundles or hair cell innervation

The $Mir182^{ko}$ heterozygotes have audiograms which resemble the wildtype, while the homozygotes exhibit mild hearing loss at the higher frequencies, more severe and earlier in onset than the progressive high-frequency hearing loss observed at later ages in the wildtype mice associated with the C57BL/6 genetic background (Fig 1). No difference in hair cell stereocilia bundles, innervation or synapse counts was observed between the $Mir182^{ko}$ wildtype, heterozygous and homozygous mice at P28 (Fig EV1, EV2, Fig 5), but at that age $Mir182^{ko}$ homozygotes still have normal hearing. However, even at P56, when $Mir182^{ko}$ homozygotes exhibit high frequency hearing loss, the hair cells appear unaffected (Fig 4). This is a completely different phenotype from either the $Mir96^{Dmdo}$ or the $Mir183/96^{dko}$ mice. This may explain the paucity of significantly misregulated genes in the RNA-seq data, which were obtained from P4 organs of Corti, an age chosen based on our previous work on $Mir96^{Dmdo}$ (Lewis et al, 2009). This may be too early to see much effect of the absence of miR-182 on the transcriptome. The lack of significantly enriched heptamers corresponding to the miR-182 seed region in the Sylamer analysis for miR-182 also supports this hypothesis. It is possible that the network drawn from the $Mir182^{ko}$ transcriptome shows the start of the misregulation cascade due to the microRNA knockout, but further studies at a later stage would be required for confirmation.

Relevance to human *MIR96* mutations

In this study we have shown that the phenotype of mice lacking miR-96 entirely is less severe than that of mice carrying a point mutation in the miR-96 seed region. Mice heterozygous for the $Mir183/96^{dko}$ allele display no auditory or structural phenotype when compared to wildtypes, while $Mir96^{Dmdo}$ heterozygotes have rapid, severe progressive hearing loss and disorganised stereocilia bundles. In our first study of the diminuendo point mutation, we concluded that the phenotype caused by the mutant miR-96 was mostly the result of loss of normal miR-96 targets, because all three mutations described (two in humans and one in the mouse) resulted in hearing loss (Lewis et al, 2009; Mencia et al, 2009). Our data from this study, however, suggest that the gain of novel

bioRxiv preprint doi: https://doi.org/10.1101/579003; this version posted March 16, 2019. The copyright holder for this preprint (which was not certified by peer review) is the author/funder, who has granted bioRxiv a license to display the preprint in perpetuity. It is made available under aCC-BY 4.0 International license.

targets also plays an important role in the phenotype caused by mutations in miR-96. This has important implications for understanding the effect of mutant microRNAs in the human population. So far all three reported human mutations in miR-96 have been point mutations, two in the seed region and one in the stem region of the pre-miRNA (Mencia et al, 2009; Solda et al, 2012), and while all the individuals carrying those point mutations have exhibited some degree of progressive hearing loss, the phenotypes differ between people, as do the phenotypes of the mice carrying the *Mir96*^{Dmdo} mutation and the *Mir183/96*^{dko} allele. Determining the misregulated pathways common to all *Mir96* mutations will be important not only for furthering our understanding of the role of this microRNA in hair cell development but also for developing therapeutic interventions.

A new bioinformatic analysis tool

Our network tool (PoPCoRN) makes use of publicly available data to draw a causal network of potential regulatory interactions which could explain the observed misregulation. Similar approaches have been described previously (Chindelevitch et al, 2012; Fakhry et al, 2016; Kramer et al, 2014; Pollard et al, 2005), but they address the case where the upstream regulator or regulators remain unknown, for example when comparing samples from healthy and diseased tissues, and one of their main aims is to identify potential upstream regulators. Our implementation asks a different question, exploring the regulatory cascade of a known regulator. In the case of miR-96, and potentially many other regulators involved in disease, the genes involved in mediating their effect are candidate therapeutic targets.

Methods

Ethics approval: Mouse studies were carried out in accordance with UK Home Office regulations and the UK Animals (Scientific Procedures) Act of 1986 (ASPA) under UK Home Office licences, and the study was approved by both the Wellcome Trust Sanger Institute and the King's College London Ethical Review Committees. Mice were culled using methods approved under these licences to minimize any possibility of suffering.

Mice. The miR-183/96 and miR-182 knockouts in C57BL/6N derived JM8.A3 ES cells were generated as previously described (Prosser et al, 2011). On chromosome 6 regions 30169424bp to 30169772bp (NCBIM38) for miR-182 and 30169424bp to 30169772bp (NCBIM38) for miR-183/96 were replaced with the PuroΔTK selection cassette. For both knockouts the PuroΔtk gene was subsequently deleted by transient transfection with Cre recombinase leading to recombination of the loxP sites that flanked the selection marker under 2-Fluoro-2-deoxy-1D-arabinofuranosyl-5-iodouracil (FIAU) selection. Heterozygous targeted ES cells were microinjected into C57BL/6N embryos for chimaera production. Mice were maintained on a C57BL/6N background . Both lines are available through EMMA (*Mir183/96*^{dko} mice: EM:10856; *Mir182*^{ko} mice: EM:12223).

Auditory Brainstem Response. The hearing of *Mir183/96*^{dko} and *Mir182*^{ko} homozygote, heterozygote and wildtype littermates was tested using the Auditory Brainstem Response, following the protocol described in (Ingham et al, 2011). Animals were sedated using a ketamine/xylazine mix (10mg ketamine and 0.1mg xylazine in 0.1ml per 10g body weight) and recovered where possible using atipamezole (0.01mg atipamezole in 0.1ml per 10g body weight) to enable recurrent testing of the same cohort of mice. All injections were intraperitoneal. Responses were recorded from three subcutaneous needle electrodes placed one over the left bulla (reference), one over the right bulla

bioRxiv preprint doi: https://doi.org/10.1101/579003; this version posted March 16, 2019. The copyright holder for this preprint (which was not certified by peer review) is the author/funder, who has granted bioRxiv a license to display the preprint in perpetuity. It is made available under aCC-BY 4.0 International license.

(ground) and one on the vertex (active). We used a broadband click stimulus and 3kHz, 6kHz, 12kHz, 18kHz, 24kHz, 30kHz, 36kHz and 42kHz pure tone frequencies, at sound levels from 0-95dB, in 5dB steps. 256 stimulus presentations per frequency were carried out per frequency and sound level, and responses were averaged to produce the ABR waveform. The threshold for each stimulus, the lowest intensity at which a waveform could be distinguished visually, was identified using a stack of response waveforms. Mice were tested at 14 days old (P14), P21, P28 ±1 day, P56 ±2 days, P90 ±2 days and P180 ±3 days. Any hyperactivity was noted prior to anaesthesia. Wave 1 amplitudes were calculated using ABR Notebook software (courtesy of MC Liberman, Harvard Medical School/Massachusetts Eye and Ear).

Distortion Product Otoacoustic Emission (DPOAE) measurements. We measured DPOAEs in mice aged 8 weeks old, anaesthetised with an intraperitoneal injection of 0.1ml / 10g of a solution of 20% urethane. Experiments were performed using Tucker Davis Technologies (TDT) BioSigRZ software driving a TDT RZ6 auditory processor and a pair of TDT MF1 magnetic loudspeakers. Signals were recorded via an Etymotic ER-10B+ low-noise DPOAE microphone. Stimulus tones (f1 & f2) were presented and microphone signals recorded via a closed-field acoustic system sealed into the auditory meatus of the mouse. Stimulus tones were presented at an f2:f1 ratio of 1.2. f2 tones were presented at frequencies to match ABR measurements (6, 12, 18, 24, 30 and 36 kHz). f1 was presented at levels from 0–85 dB in 5dB steps. f2 was presented at 10 dB below the level of f1. The magnitude of the 2f1-f2 DPOAE component was extracted from a fast Fourier transform of the recorded microphone signal and plotted as a function of f2 level. For each f2 level, the 20 spectral line magnitudes surrounding the 2f1-f2 frequency were averaged to form a mean noise floor estimate for each measurement. DPOAE threshold was defined as the lowest f2 stimulus level where the emission magnitude exceeded 2 standard deviations above the mean noise floor.

Noise exposure. Wildtype and heterozygous *Mir183/96*^{dko} mice (P55±1 day) were subjected to an 8-16kHz octave-band noise at 96dB SPL for two hours while awake and unrestrained in separate small cages within an exposure chamber designed to provide a uniform sound field (for chamber details, see (Holme & Steel, 2004)). Band pass noise was generated digitally using TDT RPvdsEx software, converted to an analogue signal using a TDT RZ6 auditory processor, and amplified using a Brüel and Kjær Type 2716C power amplifier. It was delivered to a compression driver (JBL 2446H, Northridge, CA) connected to a flat front biradial horn (JBL 2380A, Northridge, CA) secured to the roof of the sound box. ABRs were carried out the day before, and 1, 3, 7, 14 and 28 days after the noise exposure. Unexposed littermates were used as controls and went through the same set of ABR measurements.

Genotyping. *Mir183/96*^{dko} knockout mice were genotyped by PCR analysis using primers spanning the introduced deletion (Appendix Table S2). The wildtype band is 841bp and the mutant band 645bp. *Mir182*^{ko} mice were genotyped in a similar fashion with one of two primer sets (Appendix Table S2). The wildtype band for the first set is 495bp and the mutant band 457bp. The wildtype band for the second set is 247bp, and the mutant band is 209bp.

Scanning electron microscopy. The inner ears of wildtype, heterozygote and homozygote mice at P28 (*Mir183/96*^{dko}, *Mir182*^{ko}) and P56 (*Mir182*^{ko}) were fixed in 2.5% glutaraldehyde in 0.1M sodium cacodylate buffer with 3mM $CaCl_2$ at room temperature for two hours. Cochleae were finely dissected in PBS and processed according to the OTOTO method (Hunter-Duvar, 1978). Samples

bioRxiv preprint doi: https://doi.org/10.1101/579003; this version posted March 16, 2019. The copyright holder for this preprint (which was not certified by peer review) is the author/funder, who has granted bioRxiv a license to display the preprint in perpetuity. It is made available under aCC-BY 4.0 International license.

were dehydrated using an ethanol series, critical point dried and mounted for examination. Low resolution images were taken to identify the 12kHz region of the cochlea (using the frequency-place map described by Müller et al (Muller et al, 2005)). Higher-resolution images were taken using a JEOL JSM 7800 Prime scanning electron microscope under a standard magnification (60x) to show the whole organ of Corti, and at higher magnifications to examine hair cell rows (2000x) and individual hair cells (15000-23000x). Whole images have been adjusted in Photoshop to normalise dynamic range across all panels, and rotated where necessary to present a uniform orientation.

Wholemount immunostaining and confocal microscopy. The cochleae of P28 mice were fixed in 4% paraformaldehyde in PBS, washed in PBS, and decalcified in 10x ethylenediaminetetraacetic acid (EDTA) for 2 hours. After fine dissection, samples were blocked in 5% normal horse serum (NHS), 1% bovine serum albumin (BSA) and 0.3% Triton X-100 in PBS for 45 minutes at room temperature, then immunostained in 1% NHS and 0.3% Triton X-100 in PBS, as described in (Buniello et al, 2016). The primary antibodies used were anti-NFH (Abcam, cat. no: ab4680, diluted 1:800), anti-GluR2 (Millipore, cat. no: MAB397, diluted 1:200) and anti-Ribeye (Synaptic Systems, cat. no: 192 103, diluted 1:500), and the secondary antibodies were Alexa Fluor 488 goat anti-chicken (Invitrogen, cat. no: A11039, diluted 1:300), Alexa Fluor 546 goat anti-rabbit (Invitrogen, cat. no: A11035, diluted 1:300) and Alexa Fluor 488 goat anti-mouse (Invitrogen, cat. no: A21131, diluted 1:300). Samples were mounted in ProLong Gold antifade mounting medium with DAPI (Life Technologies, cat. no: P36931), or Vectashield Mounting Medium with DAPI (Vector Laboratories, cat. no: H-1200), and imaged with a Zeiss Imager 710 confocal microscope (plan-APOCHROMAT 63x Oil DIC objective) interfaced with ZEN 2010 software, or a Nikon A1R point-scanning confocal microscope (Plan Apo VC 60x/1.4NA oil objective) using NIS Elements v4.2 software (Nikon Instruments UK). Confocal z-stacks were obtained with a z-step size of 0.25µm (for synapses) or 0.4µm (for innervation). For synapse counting, a low magnification image was taken of approximately 20 inner hair cells in the 12kHz region, then a close-up image (2.5x optical zoom) was taken from both extremes of the low magnification image to ensure no synapses were counted twice. Synapses were counted from the maximum projection of the close up images using the FIJI plugin of ImageJ, and divided by the number of hair cell nuclei visible in the field of view (between 5 and 13, depending on which microscope was used) to obtain the number of synapses/hair cell. Where synapses were counted in both ears from the same mouse, the count was averaged before inclusion in the data. Whole images were processed in Adobe Photoshop, rotated where necessary, and adjusted so that all channels were equally visible.

Dissection and RNA extraction. The organs of Corti of four-day-old (P4) mice were dissected during a fixed time window (between 6 and 7.5 hours after lights on) to avoid circadian variation, and stored at -20°C in RNAlater stabilisation reagent (Ambion). RNA was extracted from both organs of Corti using either QIAshredder columns (QIAgen, cat. no. 79654) and the RNeasy mini kit (QIAgen, cat. no. 74104), or the Lexogen SPLIT kit (Lexogen, cat. no. 008.48), following the manufacturer's instructions. RNA concentration was measured using a Nanodrop spectrophotometer (ND-8000).

RNA-seq. RNA from both ears of six wildtype and six sex-matched homozygote mutant littermates from each mutant line were used for RNA-seq. Samples were not pooled. Strand-specific libraries were prepared using the NuGEN Ovation Mouse RNA-Seq System 1-16 kit (NuGEN, cat. no. 0348) and sequenced on an Illumina HiSeq 2500 machine as paired-end 125bp reads. The resulting reads were quality checked using FastQC 0.11.4 and trimmed with Trimmomatic 0.35 (Bolger et al, 2014);

bioRxiv preprint doi: https://doi.org/10.1101/579003; this version posted March 16, 2019. The copyright holder for this preprint (which was not certified by peer review) is the author/funder, who has granted bioRxiv a license to display the preprint in perpetuity. It is made available under aCC-BY 4.0 International license.

adapters were removed, trailing ends were clipped where the quality was low and a sliding window approach used to control for quality across the entire read. Finally, reads with 36 basepairs or fewer were discarded, because the shorter a read, the less likely it is to map uniquely to the genome. Reads were assembled to GRCm38 using Hisat2 version 2.0.2beta (Kim et al, 2015). Bam files were soft-clipped beyond end-of-reference alignments and MAPQ scores set to 0 for unmapped reads using Picard 2.1.0 (Broad Institute, Cambridge, Mass. http://broadinstitute.github.io/picard) and checked for quality using QoRTS (Hartley & Mullikin, 2015). The QoRTS tool also generates count data (in the same format as HTSeq), and these were used with edgeR (Robinson et al, 2010) to carry out a generalized linear model likelihood ratio test. Splicing analyses were performed using Cuffdiff (Cufflinks)(Trapnell et al, 2010), JunctionSeq(Hartley & Mullikin, 2016) and Leafcutter(Li et al, 2016).

Transcriptome and network analysis. Sylamer 10-188 (van Dongen et al, 2008) was used to examine genes ranked in order of their misregulation from up- to downregulated for over- and under-represented heptamers in their 3' UTRs. Ingenuity Pathway Analysis (IPA) was used to generate potential upstream regulators for the affected genes, using the causal network analysis module.

RTPCR and qPCR. Organ of Corti RNA was normalised to the same concentration within each litter, then treated with DNAse 1 (Sigma, cat. no: AMPD1) before cDNA creation. cDNA was made using Superscript II Reverse Transcriptase (Invitrogen, cat. no: 11904-018) or M-MLV Reverse Transcriptase (Invitrogen, cat. no: 28025-013) or Precision Reverse Transcription Premix (PrimerDesign, cat. no: RT-premix2). MicroRNA cDNA was made using the miRCURY LNA RT Kit (QIAGEN, cat. no: 339340). Primers for sequencing cDNA for testing differential splicing were designed using Primer3(Untergasser et al, 2012) (Appendix Table S2). Sanger sequencing was carried out by Source Bioscience and analysed using Gap4(Bonfield et al, 1995). Quantitative RT-PCR was carried out on a CFX Connect qPCR machine (Bio-Rad), using probes from Applied Biosystems and QIAGEN (see Appendix Table S2 for primer/probe details) and Sso-Advanced Master Mix (Bio-Rad, cat. no: 1725281) or the miRCURY LNA SYBR Green PCR Kit (QIAGEN, cat. no: 339345) for miRNA qPCR. Relative expression levels were calculated using the $2^{-\Delta\Delta ct}$ equation (Livak & Schmittgen, 2001), with *Hprt* as an internal control for all protein-coding genes except *Ocm* and *Slc26a5*, which are specifically expressed in hair cells, for which *Jag1* was used as an internal control, because it is expressed in supporting cells of the organ of Corti (Morrison et al, 1999; Zine et al, 2000). For all other genes and microRNAs, the quantity of sensory tissue present was checked using *Jag1*, and pairs were only used if their *Jag1* levels did not differ by more than ±20%. For the microRNA qPCR, the internal control was *Mir99a*, which is expressed in most cell types in the cochlea (Friedman et al, 2009). At least three technical replicates of each sample were carried out for each reaction, and at least four biological replicates were tested per probe (see legends of Fig EV3 and Appendix Fig 7 for numbers for each probe).

Statistics. For qPCR and synapse counts, the Wilcoxon rank sum test was chosen to determine significance, because it is a suitable test for small sample sizes and populations of unknown characteristics (Bridge & Sawilowsky, 1999). For repeated ABR threshold analyses, the thresholds were not normally distributed, so the data were first transformed using the arcsine transformation then analysed using separate linear models for each frequency with a compound symmetric covariance structure and restricted Maximum Likelihood Estimation (Duricki et al, 2016). This allowed the inclusion of all available data, unlike the repeated measures ANOVA, which requires the discarding of a subject if any data points are missed (for example, if a mouse died before the final

bioRxiv preprint doi: https://doi.org/10.1101/579003; this version posted March 16, 2019. The copyright holder for this preprint (which was not certified by peer review) is the author/funder, who has granted bioRxiv a license to display the preprint in perpetuity. It is made available under aCC-BY 4.0 International license.

ABR measurement) (Krueger & Tian, 2004). For each stimulus the double interaction of genotype and age was measured, followed by Bonferroni correction for multiple testing. Wilcoxon rank sum tests were carried out using R, and the arcsine transformation and mixed model linear pairwise comparison were done with SPSS v25.

Immunohistochemistry. Samples from P4 pups were collected, fixed in 10% formalin, embedded in paraffin wax and cut into 8µm sections. Immunohistochemistry was carried out using a Ventana Discovery machine and reagents according to the manufacturer's instructions (DABMap^{TM} Kit (cat.no 760-124), Hematoxylin (cat.no 760-2021), Bluing reagent (cat.no 760-2037), CC1 (cat.no 950-124), EZPrep (cat.no 950-100), LCS (cat.no 650-010), RiboWash (cat.no 760-105), Reaction Buffer (cat.no 95-300), and RiboCC (cat.no 760-107)). For each antibody, at least three wildtype/homozygote littermate pairs were tested, and from each animal, at least five mid-modiolar sections were used per antibody. Primary antibodies used were rabbit anti-Ocm (Abcam, cat. no: ab150947, diluted 1:50) and goat anti-Prestin (*Slc26a5*) (Santa Cruz, cat. no: sc-22692, diluted 1:50), and secondary antibodies were anti-goat (Jackson ImmunoResearch, cat.no 705-065-147, diluted 1:100), and anti-rabbit (Jackson ImmunoResearch, cat.no 711-065-152, diluted 1:100). Antibodies were diluted in staining solution (10% foetal calf serum, 0.1% Triton, 2% BSA and 0.5% sodium azide in PBS). A Zeiss Axioskop 2 microscope with a Plan Neofluar 63x 1.4NA objective was used to examine slides, and photos were taken using a Zeiss Axiocam camera and the associated Axiocam software. Images were processed in Adobe Photoshop; minimal adjustments were made, including rotation and resizing. Where image settings were altered, the adjustment was applied equally to wildtype and mutant photos and to the whole image.

Prediction of potential causal regulatory networks. In our previous analysis (Lewis et al, 2016), we used interactions from the literature to connect miR-96 to as many of the misregulated genes in *Mir96*^{Dmdo} homozygotes as possible. In order to automate this procedure, a custom script (prediction of potential causal regulatory networks, PoPCoRN) was written to make use of publically available regulatory data from ArrayExpress and the associated Expression Atlas (Kolesnikov et al, 2015; Petryszak et al, 2016), OregAnno (Lesurf et al, 2016), miRTarBase (Chou et al, 2016), TransmiR (Wang et al, 2010) and TRRUST (Han et al, 2015) (table 2). All these data are based on experimental evidence, although we did make use of human regulatory interactions by converting human gene IDs to mouse gene IDs where there was a one-to-one orthologue (using Ensembl). Interactions from our previous network (Lewis et al, 2016), which were obtained from the literature using Ingenuity IPA, were also added, as were regulations reported in (Hertzano et al, 2007), which is not available through ArrayExpress but is a particularly relevant study, since it reports the results of microarrays carried out on RNA from mouse inner ears. MicroRNA targets confirmed in the literature were included, as were experimentally validated targets listed in miRTarBase as having “strong experimental evidence”, either reporter assay or Western blot (Chou et al, 2016), and genes predicted or confirmed to be miR-96 targets by our previous studies (Lewis et al, 2016; Lewis et al, 2009). Finally, genes upregulated in *Mir183/96*^{dko} homozygotes with heptamers complementary to either the miR-96 or the miR-183 seed region in their 3’UTR were included as targets of the relevant microRNA(s) (Table EV1, top). Similarly, genes upregulated in *Mir182*^{ko} homozygotes with heptamers complementary to the miR-182 seed region in their 3’UTR were included as targets of miR-182 (Table EV1, bottom). This resulted in a list of 64438 unique links of the form <gene A> <interaction> <gene B>.

bioRxiv preprint doi: https://doi.org/10.1101/579003; this version posted March 16, 2019. The copyright holder for this preprint (which was not certified by peer review) is the author/funder, who has granted bioRxiv a license to display the preprint in perpetuity. It is made available under aCC-BY 4.0 International license.

Table 2 Data used as a basis for building the regulatory networks.

Database	Format example	Entries	Reference
ArrayExpress and the Gene Expression Atlas	If a null allele of gene A results in a decrease in expression of gene B, gene A upregulates gene B	75686	(Kolesnikov et al, 2015; Petryszak et al, 2016)
ORegAnno	If there is a binding site in gene B for gene A, and the outcome of the interaction is NEGATIVE, gene A downregulates gene B	5394	(Lesurf et al, 2016)
miRTarBase	If microRNA X has target gene A, X downregulates A	860	(Chou et al, 2016)
TransmiR	If gene A represses microRNA X, A downregulates X	19	(Wang et al, 2010)
TRRUST	If the relationship between gene A and gene B is activation, gene A upregulates gene B	4460	(Han et al, 2015)
n/a	Various	519	(Hertzano et al, 2007; Lewis et al, 2016)
n/a	If a null allele of microRNA X results in an increase in expression of gene A, and gene A has seed region matches for X, microRNA X downregulates gene A	18	Current study

All potential links between the ultimate regulators (*Mir183* and *Mir96*, or *Mir182*) and the misregulated genes were then identified, and the direction of misregulation of intermediate genes predicted. Starting with the known misregulated genes, each upstream regulator was given a score based on the direction of regulation of the known misregulated genes (Fig EV4). This process iterated until the gene(s) at the top of the cascade (in this case, *Mir96*, *Mir183* or *Mir182*) were reached. Consistent links were kept, the shortest paths between microRNA and misregulated genes identified, and the final network was written out in the simple interaction format (sif) and viewed using Cytoscape (Shannon et al, 2003) (Fig EV4).

Strain differences in seed region matches. The C57BL/6NJ genomic sequence is available from the Mouse Genomes Project (Adams et al, 2015) via the Ensembl browser (Zerbino et al, 2018), but the *Mir96*^{Dmdo} mice were made and maintained on the C3HeB/FeJ background, which is not one of the sequenced strains. Instead, we made use of genomic sequence from the C3H/HeJ strain, which is closely related to C3HeB/FeJ and is one of the other strains sequenced as part of the Mouse

bioRxiv preprint doi: https://doi.org/10.1101/579003; this version posted March 16, 2019. The copyright holder for this preprint (which was not certified by peer review) is the author/funder, who has granted bioRxiv a license to display the preprint in perpetuity. It is made available under aCC-BY 4.0 International license.

Genomes Project. We searched the 3'UTRs of each strain for the complement of the miR-96 seed region (GTGCCAA). We removed genes without an MGI ID, since without a consistent ID the corresponding gene in the other strain could not be identified. 1733 genes were left with at least one match to the miR-96 seed region in their 3' UTRs in one or both strains. 21 genes had no 3'UTR sequence available for C57BL/6NJ, and 31 genes had no 3'UTR sequence available for C3H/HeJ.

Declarations

Ethics approval: Mouse studies were carried out in accordance with UK Home Office regulations and the UK Animals (Scientific Procedures) Act of 1986 (ASPA) under UK Home Office licences, and the study was approved by both the Wellcome Trust Sanger Institute and the King's College London Ethical Review Committees. Mice were culled using methods approved under these licences to minimize any possibility of suffering.

Consent for publication: Not applicable.

Data and software availability:

The datasets and computer code produced in this study are available in the following databases:

- RNA-Seq data: ArrayExpress E-MTAB-5800 (https://www.ebi.ac.uk/arrayexpress/experiments/E-MTAB-5800).
- PoPCoRN network construction script: GitHub (https://github.com/moraglewis/PoPCoRN)

Conflicts of interest: The authors declare that they have no conflicts of interest.

Funding: This project was supported by Action on Hearing Loss (Pauline Ashley Fellowship to MAL), the MRC (KPS, MC_qA137918, G0300212) and the Wellcome Trust (098051, KPS: 100699). The Zeiss Imager Confocal Microscope is maintained with a Wellcome Trust grant (WT089622MA). No role was taken by any funding body in designing the study, in collection, analysis or interpretation of data, or in the writing of this manuscript.

Authors' contributions: M.A.L. carried out the ABR, noise exposure, organ of Corti dissection, RNA extraction, transcriptome analysis, cDNA creation, mRNA qPCR, Sanger sequencing and immunohistochemistry. F.D.D. performed the wholemount dissections, scanning electron microscopy, immunostaining, confocal microscopy, RNA extraction, cDNA creation and microRNA qPCR. DPOAEs were carried out by N.J.I. M.A.L. wrote and tested the PoPCoRN perl script. H.M.P. generated the *Mir183/96*^{dko} and *Mir182*^{ko} knockout mice. The study was designed and the paper was written by M.A.L. and K.P.S. and reviewed by all authors.

Acknowledgements: The RNA-Seq was carried out by the National Institute for Health Research (NIHR) Biomedical Research Centre based at Guy's and St Thomas' NHS Foundation Trust and King's College London. We thank Matthew Arno and Sucharitha Balu for doing the RNA library preps and sample submission. The confocal microscopy was carried out with help from the Nikon Imaging Centre at Kings College London, and the scanning electron microscopy was done at the King's College London Centre for Ultrastructural Imaging. We are grateful to Allan Bradley for access to the *Mir183/96*^{dko} and *Mir182*^{ko} mice. We thank Holly Smith for her work on the immunohistochemistry.

bioRxiv preprint doi: https://doi.org/10.1101/579003; this version posted March 16, 2019. The copyright holder for this preprint (which was not certified by peer review) is the author/funder, who has granted bioRxiv a license to display the preprint in perpetuity. It is made available under aCC-BY 4.0 International license.

References

Adams DJ, Doran AG, Lilue J, Keane TM (2015) The Mouse Genomes Project: a repository of inbred laboratory mouse strain genomes. *Mamm Genome* **26:** 403-412

Andrews S (2010) FastQC: a quality control tool for high throughput sequence data. http://www.bioinformatics.babraham.ac.uk/projects/fastqc/.

Barreau C, Paillard L, Osborne HB (2005) AU-rich elements and associated factors: are there unifying principles? *Nucleic Acids Res* **33:** 7138-7150

Bolger AM, Lohse M, Usadel B (2014) Trimmomatic: a flexible trimmer for Illumina sequence data. *Bioinformatics* **30:** 2114-2120

Bonfield JK, Smith K, Staden R (1995) A new DNA sequence assembly program. *Nucleic Acids Res* **23:** 4992-4999

Boutz PL, Chawla G, Stoilov P, Black DL (2007) MicroRNAs regulate the expression of the alternative splicing factor nPTB during muscle development. *Genes Dev* **21:** 71-84

Bridge PD, Sawilowsky SS (1999) Increasing physicians' awareness of the impact of statistics on research outcomes: comparative power of the t-test and and Wilcoxon Rank-Sum test in small samples applied research. *J Clin Epidemiol* **52:** 229-235

Buniello A, Ingham NJ, Lewis MA, Huma AC, Martinez-Vega R, Varela-Nieto I, Vizcay-Barrena G, Fleck RA, Houston O, Bardhan T, Johnson SL, White JK, Yuan H, Marcotti W, Steel KP (2016) Wbp2 is required for normal glutamatergic synapses in the cochlea and is crucial for hearing. *EMBO Mol Med* **8:** 191-207

Cai T, Jen HI, Kang H, Klisch TJ, Zoghbi HY, Groves AK (2015) Characterization of the transcriptome of nascent hair cells and identification of direct targets of the Atoh1 transcription factor. *J Neurosci* **35:** 5870-5883

Chen CY, Shyu AB (1995) AU-rich elements: characterization and importance in mRNA degradation. *Trends Biochem Sci* **20:** 465-470

Chen J, Johnson SL, Lewis MA, Hilton JM, Huma A, Marcotti W, Steel KP (2014) A reduction in Ptprq associated with specific features of the deafness phenotype of the miR-96 mutant mouse diminuendo. *Eur J Neurosci* **39:** 744-756

Chervenak AP, Bank LM, Thomsen N, Glanville-Jones HC, Jonathan S, Millen KJ, Arkell RM, Barald KF (2014) The role of Zic genes in inner ear development in the mouse: Exploring mutant mouse phenotypes. *Dev Dyn* **243:** 1487-1498

bioRxiv preprint doi: https://doi.org/10.1101/579003; this version posted March 16, 2019. The copyright holder for this preprint (which was not certified by peer review) is the author/funder, who has granted bioRxiv a license to display the preprint in perpetuity. It is made available under aCC-BY 4.0 International license.

Chindelevitch L, Ziemek D, Enayetallah A, Randhawa R, Sidders B, Brockel C, Huang ES (2012) Causal reasoning on biological networks: interpreting transcriptional changes. *Bioinformatics* **28:** 1114-1121

Chou CH, Chang NW, Shrestha S, Hsu SD, Lin YL, Lee WH, Yang CD, Hong HC, Wei TY, Tu SJ, Tsai TR, Ho SY, Jian TY, Wu HY, Chen PR, Lin NC, Huang HT, Yang TL, Pai CY, Tai CS et al (2016) miRTarBase 2016: updates to the experimentally validated miRNA-target interactions database. *Nucleic Acids Res* **44:** D239-247

Duricki DA, Soleman S, Moon LD (2016) Analysis of longitudinal data from animals with missing values using SPSS. *Nat Protoc* **11:** 1112-1129

Elkon R, Milon B, Morrison L, Shah M, Vijayakumar S, Racherla M, Leitch CC, Silipino L, Hadi S, Weiss-Gayet M, Barras E, Schmid CD, Ait-Lounis A, Barnes A, Song Y, Eisenman DJ, Eliyahu E, Frolenkov GI, Strome SE, Durand B et al (2015) RFX transcription factors are essential for hearing in mice. *Nat Commun* **6:** 8549

Erichsen S, Stierna P, Bagger-Sjoback D, Curtis LM, Rarey KE, Schmid W, Hultcrantz M (1998) Distribution of Na,K-ATPase is normal in the inner ear of a mouse with a null mutation of the glucocorticoid receptor. *Hear Res* **124:** 146-154

Fakhry CT, Choudhary P, Gutteridge A, Sidders B, Chen P, Ziemek D, Zarringhalam K (2016) Interpreting transcriptional changes using causal graphs: new methods and their practical utility on public networks. *BMC Bioinformatics* **17:** 318

Fan J, Jia L, Li Y, Ebrahim S, May-Simera H, Wood A, Morell RJ, Liu P, Lei J, Kachar B, Belluscio L, Qian H, Li T, Li W, Wistow G, Dong L (2017) Maturation arrest in early postnatal sensory receptors by deletion of the miR-183/96/182 cluster in mouse. *Proc Natl Acad Sci U S A* **114:** E4271-E4280

Friedman LM, Dror AA, Mor E, Tenne T, Toren G, Satoh T, Biesemeier DJ, Shomron N, Fekete DM, Hornstein E, Avraham KB (2009) MicroRNAs are essential for development and function of inner ear hair cells in vertebrates. *Proc Natl Acad Sci U S A* **106:** 7915-7920

Geng R, Furness DN, Muraleedharan CK, Zhang J, Dabdoub A, Lin V, Xu S (2018) The microRNA-183/96/182 Cluster is Essential for Stereociliary Bundle Formation and Function of Cochlear Sensory Hair Cells. *Sci Rep* **8:** 18022

Han H, Shim H, Shin D, Shim JE, Ko Y, Shin J, Kim H, Cho A, Kim E, Lee T, Kim K, Yang S, Bae D, Yun A, Kim S, Kim CY, Cho HJ, Kang B, Shin S, Lee I (2015) TRRUST: a reference database of human transcriptional regulatory interactions. *Sci Rep* **5:** 11432

Hartley SW, Mullikin JC (2015) QoRTs: a comprehensive toolset for quality control and data processing of RNA-Seq experiments. *BMC Bioinformatics* **16:** 224

bioRxiv preprint doi: https://doi.org/10.1101/579003; this version posted March 16, 2019. The copyright holder for this preprint (which was not certified by peer review) is the author/funder, who has granted bioRxiv a license to display the preprint in perpetuity. It is made available under aCC-BY 4.0 International license.

Hartley SW, Mullikin JC (2016) Detection and visualization of differential splicing in RNA-Seq data with JunctionSeq. *Nucleic Acids Res* **44:** e127

Hertzano R, Dror AA, Montcouquiol M, Ahmed ZM, Ellsworth B, Camper S, Friedman TB, Kelley MW, Avraham KB (2007) Lhx3, a LIM domain transcription factor, is regulated by Pou4f3 in the auditory but not in the vestibular system. *Eur J Neurosci* **25:** 999-1005

Holme RH, Steel KP (2004) Progressive hearing loss and increased susceptibility to noise-induced hearing loss in mice carrying a Cdh23 but not a Myo7a mutation. *J Assoc Res Otolaryngol* **5:** 66-79

Hunter-Duvar IM (1978) A technique for preparation of cochlear specimens for assessment with the scanning electron microscope. *Acto Otoloaryng Suppl* **351:** 3-23

Ingham NJ, Pearson S, Steel KP (2011) Using the Auditory Brainstem Response (ABR) to Determine Sensitivity of Hearing in Mutant Mice. *Curr Protoc Mouse Biol* **1:** 279-287

Kim D, Langmead B, Salzberg SL (2015) HISAT: a fast spliced aligner with low memory requirements. *Nat Methods* **12:** 357-360

Kolesnikov N, Hastings E, Keays M, Melnichuk O, Tang YA, Williams E, Dylag M, Kurbatova N, Brandizi M, Burdett T, Megy K, Pilicheva E, Rustici G, Tikhonov A, Parkinson H, Petryszak R, Sarkans U, Brazma A (2015) ArrayExpress update--simplifying data submissions. *Nucleic Acids Res* **43:** D1113-1116

Kramer A, Green J, Pollard J, Jr., Tugendreich S (2014) Causal analysis approaches in Ingenuity Pathway Analysis. *Bioinformatics* **30:** 523-530

Krueger C, Tian L (2004) A comparison of the general linear mixed model and repeated measures ANOVA using a dataset with multiple missing data points. *Biol Res Nurs* **6:** 151-157

Kuhn S, Johnson SL, Furness DN, Chen J, Ingham N, Hilton JM, Steffes G, Lewis MA, Zampini V, Hackney CM, Masetto S, Holley MC, Steel KP, Marcotti W (2011) miR-96 regulates the progression of differentiation in mammalian cochlear inner and outer hair cells. *Proc Natl Acad Sci U S A* **108:** 2355-2360

Kujawa SG, Liberman MC (2009) Adding insult to injury: cochlear nerve degeneration after "temporary" noise-induced hearing loss. *J Neurosci* **29:** 14077-14085

Kurima K, Peters LM, Yang Y, Riazuddin S, Ahmed ZM, Naz S, Arnaud D, Drury S, Mo J, Makishima T, Ghosh M, Menon PS, Deshmukh D, Oddoux C, Ostrer H, Khan S, Deininger PL, Hampton LL, Sullivan SL, Battey JF, Jr. et al (2002) Dominant and recessive deafness caused by mutations of a novel gene, TMC1, required for cochlear hair-cell function. *Nat Genet* **30:** 277-284

bioRxiv preprint doi: https://doi.org/10.1101/579003; this version posted March 16, 2019. The copyright holder for this preprint (which was not certified by peer review) is the author/funder, who has granted bioRxiv a license to display the preprint in perpetuity. It is made available under aCC-BY 4.0 International license.

Lalani SR, Safiullah AM, Molinari LM, Fernbach SD, Martin DM, Belmont JW (2004) SEMA3E mutation in a patient with CHARGE syndrome. *J Med Genet* **41:** e94

Lesurf R, Cotto KC, Wang G, Griffith M, Kasaian K, Jones SJ, Montgomery SB, Griffith OL (2016) ORegAnno 3.0: a community-driven resource for curated regulatory annotation. *Nucleic Acids Res* **44:** D126-132

Lewis MA, Buniello A, Hilton JM, Zhu F, Zhang WI, Evans S, van Dongen S, Enright AJ, Steel KP (2016) Exploring regulatory networks of miR-96 in the developing inner ear. *Sci Rep* **6:** 23363

Lewis MA, Quint E, Glazier AM, Fuchs H, De Angelis MH, Langford C, van Dongen S, Abreu-Goodger C, Piipari M, Redshaw N, Dalmay T, Moreno-Pelayo MA, Enright AJ, Steel KP (2009) An ENU-induced mutation of miR-96 associated with progressive hearing loss in mice. *Nat Genet* **41:** 614-618

Li HS, Borg E (1991) Age-related loss of auditory sensitivity in two mouse genotypes. *Acta Otolaryngol* **111:** 827-834

Li YI, Knowles DA, Pritchard JK (2016) LeafCutter: Annotation-free quantification of RNA splicing. *bioRxiv*

Liberman MC, Gao J, He DZ, Wu X, Jia S, Zuo J (2002) Prestin is required for electromotility of the outer hair cell and for the cochlear amplifier. *Nature* **419:** 300-304

Liu R, Loraine AE, Dickerson JA (2014) Comparisons of computational methods for differential alternative splicing detection using RNA-seq in plant systems. *BMC Bioinformatics* **15:** 364

Liu XZ, Ouyang XM, Xia XJ, Zheng J, Pandya A, Li F, Du LL, Welch KO, Petit C, Smith RJ, Webb BT, Yan D, Arnos KS, Corey D, Dallos P, Nance WE, Chen ZY (2003) Prestin, a cochlear motor protein, is defective in non-syndromic hearing loss. *Hum Mol Genet* **12:** 1155-1162

Livak KJ, Schmittgen TD (2001) Analysis of relative gene expression data using real-time quantitative PCR and the 2(T)(-Delta Delta C) method. *Methods* **25:** 402-408

Lumayag S, Haldin CE, Corbett NJ, Wahlin KJ, Cowan C, Turturro S, Larsen PE, Kovacs B, Witmer PD, Valle D, Zack DJ, Nicholson DA, Xu S (2013) Inactivation of the microRNA-183/96/182 cluster results in syndromic retinal degeneration. *Proc Natl Acad Sci U S A* **110:** E507-516

Mencia A, Modamio-Hoybjor S, Redshaw N, Morin M, Mayo-Merino F, Olavarrieta L, Aguirre LA, del Castillo I, Steel KP, Dalmay T, Moreno F, Moreno-Pelayo MA (2009) Mutations in the seed region of human miR-96 are responsible for nonsyndromic progressive hearing loss. *Nat Genet* **41:** 609-613

Morrison A, Hodgetts C, Gossler A, Hrabe de Angelis M, Lewis J (1999) Expression of Delta1 and Serrate1 (Jagged1) in the mouse inner ear. *Mech Dev* **84:** 169-172

bioRxiv preprint doi: https://doi.org/10.1101/579003; this version posted March 16, 2019. The copyright holder for this preprint (which was not certified by peer review) is the author/funder, who has granted bioRxiv a license to display the preprint in perpetuity. It is made available under aCC-BY 4.0 International license.

Muller M, von Hunerbein K, Hoidis S, Smolders JW (2005) A physiological place-frequency map of the cochlea in the CBA/J mouse. *Hear Res* **202:** 63-73

Noben-Trauth K, Zheng QY, Johnson KR (2003) Association of cadherin 23 with polygenic inheritance and genetic modification of sensorineural hearing loss. *Nat Genet* **35:** 21-23

Petryszak R, Keays M, Tang YA, Fonseca NA, Barrera E, Burdett T, Fullgrabe A, Fuentes AM, Jupp S, Koskinen S, Mannion O, Huerta L, Megy K, Snow C, Williams E, Barzine M, Hastings E, Weisser H, Wright J, Jaiswal P et al (2016) Expression Atlas update--an integrated database of gene and protein expression in humans, animals and plants. *Nucleic Acids Res* **44:** D746-752

Pittler SJ, Baehr W (1991) Identification of a nonsense mutation in the rod photoreceptor cGMP phosphodiesterase beta-subunit gene of the rd mouse. *Proc Natl Acad Sci U S A* **88:** 8322-8326

Plass M, Rasmussen SH, Krogh A (2017) Highly accessible AU-rich regions in 3' untranslated regions are hotspots for binding of regulatory factors. *PLoS Comput Biol* **13:** e1005460

Pollard J, Jr., Butte AJ, Hoberman S, Joshi M, Levy J, Pappo J (2005) A computational model to define the molecular causes of type 2 diabetes mellitus. *Diabetes Technol Ther* **7:** 323-336

Prosser HM, Koike-Yusa H, Cooper JD, Law FC, Bradley A (2011) A resource of vectors and ES cells for targeted deletion of microRNAs in mice. *Nat Biotechnol* **29:** 840-845

Robinson MD, McCarthy DJ, Smyth GK (2010) edgeR: a Bioconductor package for differential expression analysis of digital gene expression data. *Bioinformatics* **26:** 139-140

Schluter T, Berger C, Rosengauer E, Fieth P, Krohs C, Ushakov K, Steel KP, Avraham KB, Hartmann AK, Felmy F, Nothwang HG (2018) miR-96 is required for normal development of the auditory hindbrain. *Hum Mol Genet* **27:** 860-874

Shannon P, Markiel A, Ozier O, Baliga NS, Wang JT, Ramage D, Amin N, Schwikowski B, Ideker T (2003) Cytoscape: a software environment for integrated models of biomolecular interaction networks. *Genome Res* **13:** 2498-2504

Smith CL, Blake JA, Kadin JA, Richardson JE, Bult CJ (2018) Mouse Genome Database (MGD)-2018: knowledgebase for the laboratory mouse. *Nucleic Acids Res* **46:** D836-D842

Solda G, Robusto M, Primignani P, Castorina P, Benzoni E, Cesarani A, Ambrosetti U, Asselta R, Duga S (2012) A novel mutation within the MIR96 gene causes non-syndromic inherited hearing loss in an Italian family by altering pre-miRNA processing. *Hum Mol Genet* **21:** 577-585

bioRxiv preprint doi: https://doi.org/10.1101/579003; this version posted March 16, 2019. The copyright holder for this preprint (which was not certified by peer review) is the author/funder, who has granted bioRxiv a license to display the preprint in perpetuity. It is made available under aCC-BY 4.0 International license.

Soukup GA, Fritzsch B, Pierce ML, Weston MD, Jahan I, McManus MT, Harfe BD (2009) Residual microRNA expression dictates the extent of inner ear development in conditional Dicer knockout mice. *Dev Biol* **328:** 328-341

ten Cate WJ, Curtis LM, Small GM, Rarey KE (1993) Localization of glucocorticoid receptors and glucocorticoid receptor mRNAs in the rat cochlea. *Laryngoscope* **103:** 865-871

Tong B, Hornak AJ, Maison SF, Ohlemiller KK, Liberman MC, Simmons DD (2016) Oncomodulin, an EF-Hand Ca2+ Buffer, Is Critical for Maintaining Cochlear Function in Mice. *J Neurosci* **36:** 1631-1635

Trapnell C, Williams BA, Pertea G, Mortazavi A, Kwan G, van Baren MJ, Salzberg SL, Wold BJ, Pachter L (2010) Transcript assembly and quantification by RNA-Seq reveals unannotated transcripts and isoform switching during cell differentiation. *Nat Biotechnol* **28:** 511-515

Untergasser A, Cutcutache I, Koressaar T, Ye J, Faircloth BC, Remm M, Rozen SG (2012) Primer3--new capabilities and interfaces. *Nucleic Acids Res* **40:** e115

van Dongen S, Abreu-Goodger C, Enright AJ (2008) Detecting microRNA binding and siRNA off-target effects from expression data. *Nat Methods* **5:** 1023-1025

Vreugde S, Erven A, Kros CJ, Marcotti W, Fuchs H, Kurima K, Wilcox ER, Friedman TB, Griffith AJ, Balling R, Hrabe De Angelis M, Avraham KB, Steel KP (2002) Beethoven, a mouse model for dominant, progressive hearing loss DFNA36. *Nat Genet* **30:** 257-258

Walsh T, Walsh V, Vreugde S, Hertzano R, Shahin H, Haika S, Lee MK, Kanaan M, King MC, Avraham KB (2002) From flies' eyes to our ears: mutations in a human class III myosin cause progressive nonsyndromic hearing loss DFNB30. *Proc Natl Acad Sci U S A* **99:** 7518-7523

Walsh VL, Raviv D, Dror AA, Shahin H, Walsh T, Kanaan MN, Avraham KB, King MC (2011) A mouse model for human hearing loss DFNB30 due to loss of function of myosin IIIA. *Mamm Genome* **22:** 170-177

Wang J, Lu M, Qiu C, Cui Q (2010) TransmiR: a transcription factor-microRNA regulation database. *Nucleic Acids Res* **38:** D119-122

Weston MD, Pierce ML, Rocha-Sanchez S, Beisel KW, Soukup GA (2006) MicroRNA gene expression in the mouse inner ear. *Brain Res* **1111:** 95-104

Weston MD, Tarang S, Pierce ML, Pyakurel U, Rocha-Sanchez SM, McGee J, Walsh EJ, Soukup GA (2018) A mouse model of miR-96, miR-182 and miR-183 misexpression implicates miRNAs in cochlear cell fate and homeostasis. *Sci Rep* **8:** 3569

bioRxiv preprint doi: https://doi.org/10.1101/579003; this version posted March 16, 2019. The copyright holder for this preprint (which was not certified by peer review) is the author/funder, who has granted bioRxiv a license to display the preprint in perpetuity. It is made available under aCC-BY 4.0 International license.

Xu S, Witmer PD, Lumayag S, Kovacs B, Valle D (2007) MicroRNA (miRNA) transcriptome of mouse retina and identification of a sensory organ-specific miRNA cluster. *J Biol Chem* **282:** 25053-25066

Zerbino DR, Achuthan P, Akanni W, Amode MR, Barrell D, Bhai J, Billis K, Cummins C, Gall A, Giron CG, Gil L, Gordon L, Haggerty L, Haskell E, Hourlier T, Izuogu OG, Janacek SH, Juettemann T, To JK, Laird MR et al (2018) Ensembl 2018. *Nucleic Acids Res* **46:** D754-D761

Zine A, Van De Water TR, de Ribaupierre F (2000) Notch signaling regulates the pattern of auditory hair cell differentiation in mammals. *Development* **127:** 3373-3383

bioRxiv preprint doi: https://doi.org/10.1101/579003; this version posted March 16, 2019. The copyright holder for this preprint (which was not certified by peer review) is the author/funder, who has granted bioRxiv a license to display the preprint in perpetuity. It is made available under aCC-BY 4.0 International license.

Figure legends

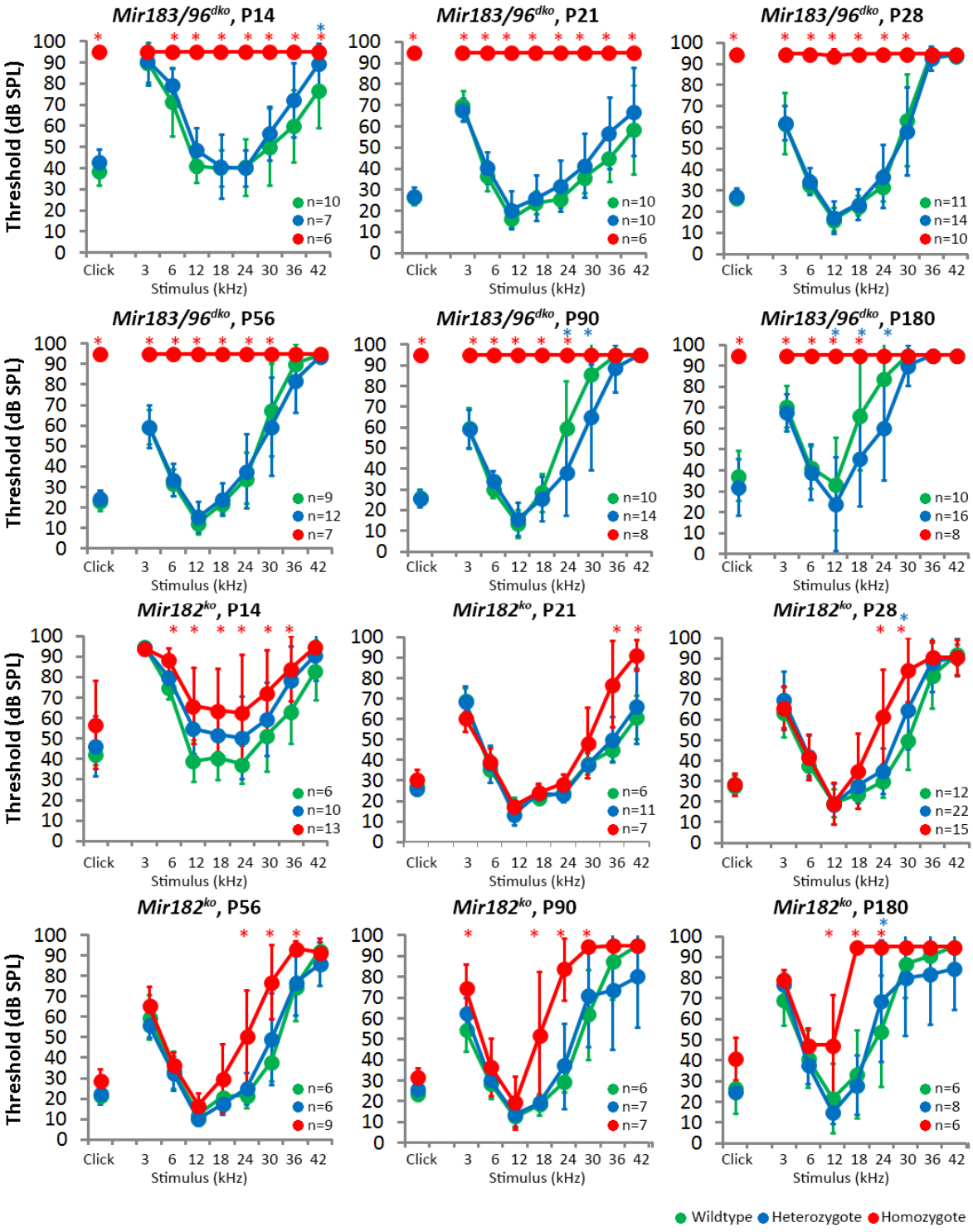

Figure 1. Mean ABR thresholds of *Mir183/96*^{dko} and *Mir182*^{ko} homozygous (red), heterozygous (blue) and wildtype (green) mice at P14, P21, P28, P56, P90 and P180. Homozygous *Mir183/96*^{dko} mice show profound hearing loss at all ages tested, and points plotted at 95dB indicate no response at this level, the maximum SPL used. Homozygous *Mir182*^{ko} mice display mildly raised thresholds at high frequencies, which slowly progresses to include the middle frequencies as the mice age.

bioRxiv preprint doi: https://doi.org/10.1101/579003; this version posted March 16, 2019. The copyright holder for this preprint (which was not certified by peer review) is the author/funder, who has granted bioRxiv a license to display the preprint in perpetuity. It is made available under aCC-BY 4.0 International license.

Heterozygotes from both lines show thresholds similar to wildtype mice. Number of mice of each genotype tested at each age is shown on the threshold plot. Error bars are standard deviation, and significant differences ($P < 0.05$, mixed linear model pairwise comparison) are marked by * in red (for a significant difference between wildtype and homozygote) or blue (for a significant difference between wildtype and heterozygote). See Appendix figures S1, S2 for individually plotted traces.

bioRxiv preprint doi: https://doi.org/10.1101/579003; this version posted March 16, 2019. The copyright holder for this preprint (which was not certified by peer review) is the author/funder, who has granted bioRxiv a license to display the preprint in perpetuity. It is made available under aCC-BY 4.0 International license.

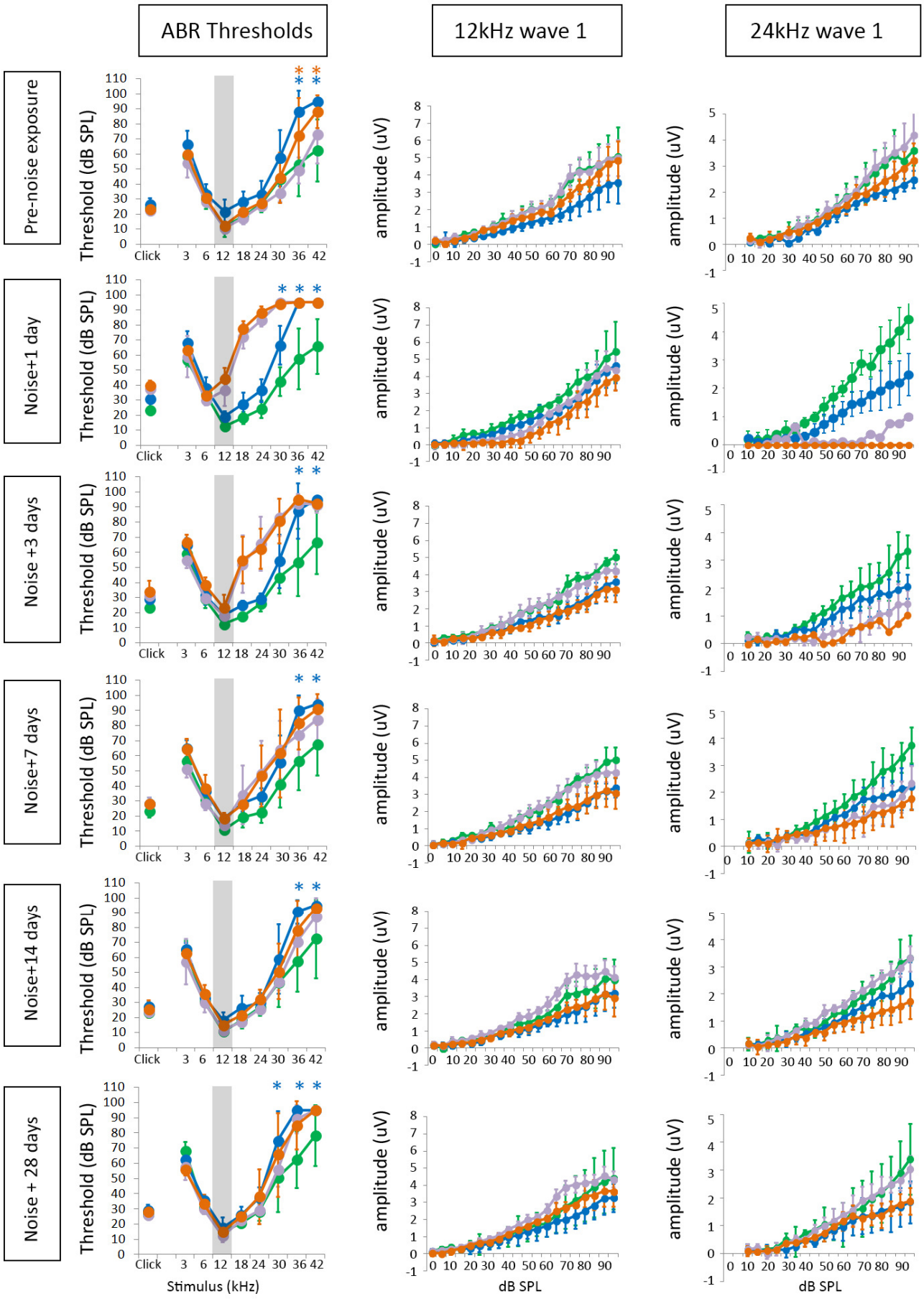

bioRxiv preprint doi: https://doi.org/10.1101/579003; this version posted March 16, 2019. The copyright holder for this preprint (which was not certified by peer review) is the author/funder, who has granted bioRxiv a license to display the preprint in perpetuity. It is made available under aCC-BY 4.0 International license.

Figure 2. Mean ABR thresholds for wildtype and heterozygous *Mir183/96*^{dko} mice subjected to noise exposure, before exposure and 1, 3, 7, 14 and 28 days after. An increase in thresholds at 12kHz and above is seen 1 day after exposure but thresholds have returned to normal by 28 days after. Significant differences ($P < 0.05$, mixed linear model pairwise comparison) are marked by * in blue (for a significant difference between wildtype unexposed mice and heterozygous unexposed mice) or orange (for a significant difference between wildtype noise-exposed mice and heterozygous noise-exposed mice). Wave 1 amplitudes at 12kHz and 24kHz are shown for each time point. No obvious effect is visible at 12kHz, but at 24kHz, one day after noise exposure, wave 1 was too poorly defined to measure the amplitude in all heterozygotes and all but one wildtype. By 28 days after exposure, both wildtype and heterozygote amplitudes have recovered to the normal range. 12 wildtype mice and 12 heterozygote mice were tested; 6 wildtypes were noise-exposed (violet) with 6 unexposed controls (green), and 6 heterozygotes were noise-exposed (orange) with 6 unexposed controls (blue). Error bars are standard deviation. The grey area on the threshold plots indicates the octave band of noise (8-16kHz).

bioRxiv preprint doi: https://doi.org/10.1101/579003; this version posted March 16, 2019. The copyright holder for this preprint (which was not certified by peer review) is the author/funder, who has granted bioRxiv a license to display the preprint in perpetuity. It is made available under aCC-BY 4.0 International license.

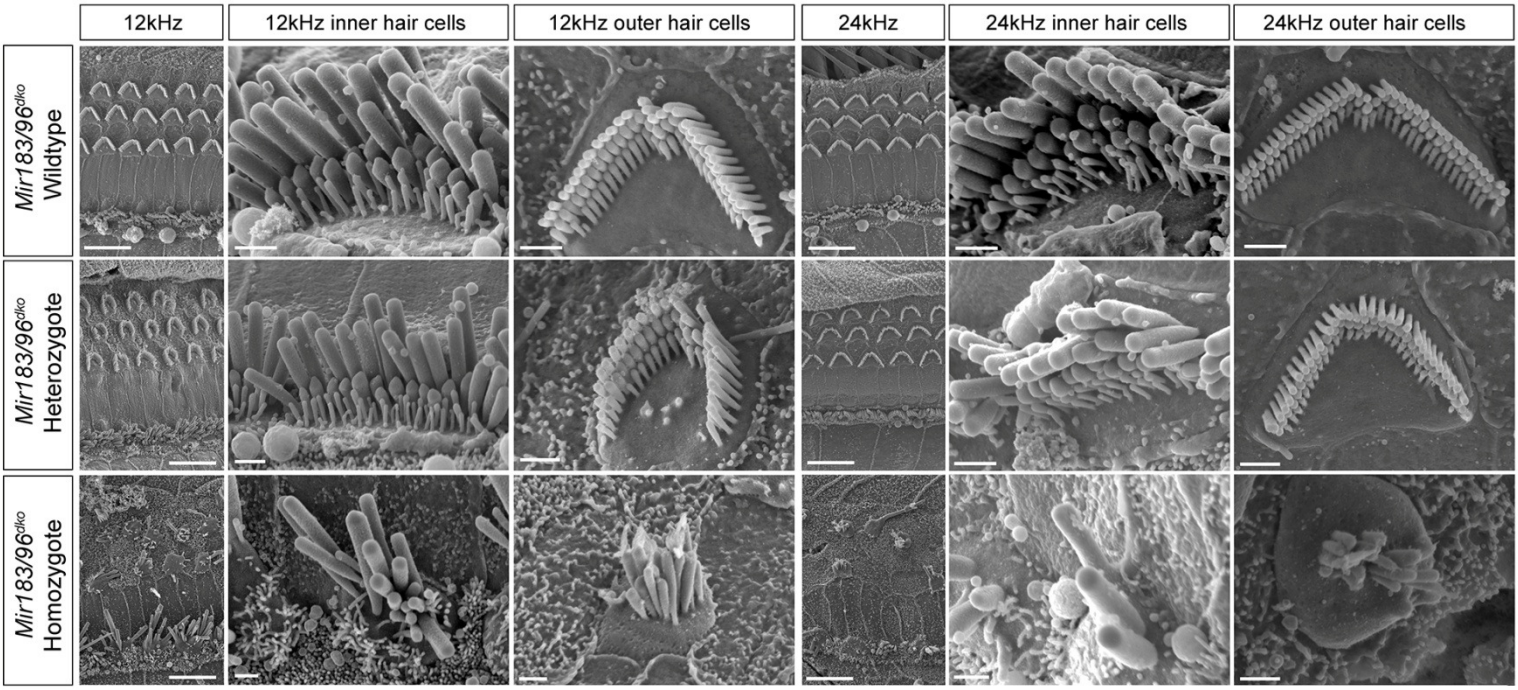

Figure 3. Scanning electron micrographs of *Mir183/96*^{dko} mice at P28. Two best-frequency regions of the organ of Corti are shown; 12kHz (68% of the way along the organ of Corti from base to apex) and 24kHz (43% of the way along the organ of Corti from base to apex). For each region, the left-hand column shows a zoomed-out image with inner and outer hair cell rows (scale bars=10µm), and the other two columns show an inner and an outer hair cell close up (scale bars=1µm). The top row shows wildtype hair cells (n=6), the middle row shows heterozygote hair cells (n=6) and the bottom row shows homozygote hair cells (n=5).

bioRxiv preprint doi: https://doi.org/10.1101/579003; this version posted March 16, 2019. The copyright holder for this preprint (which was not certified by peer review) is the author/funder, who has granted bioRxiv a license to display the preprint in perpetuity. It is made available under aCC-BY 4.0 International license.

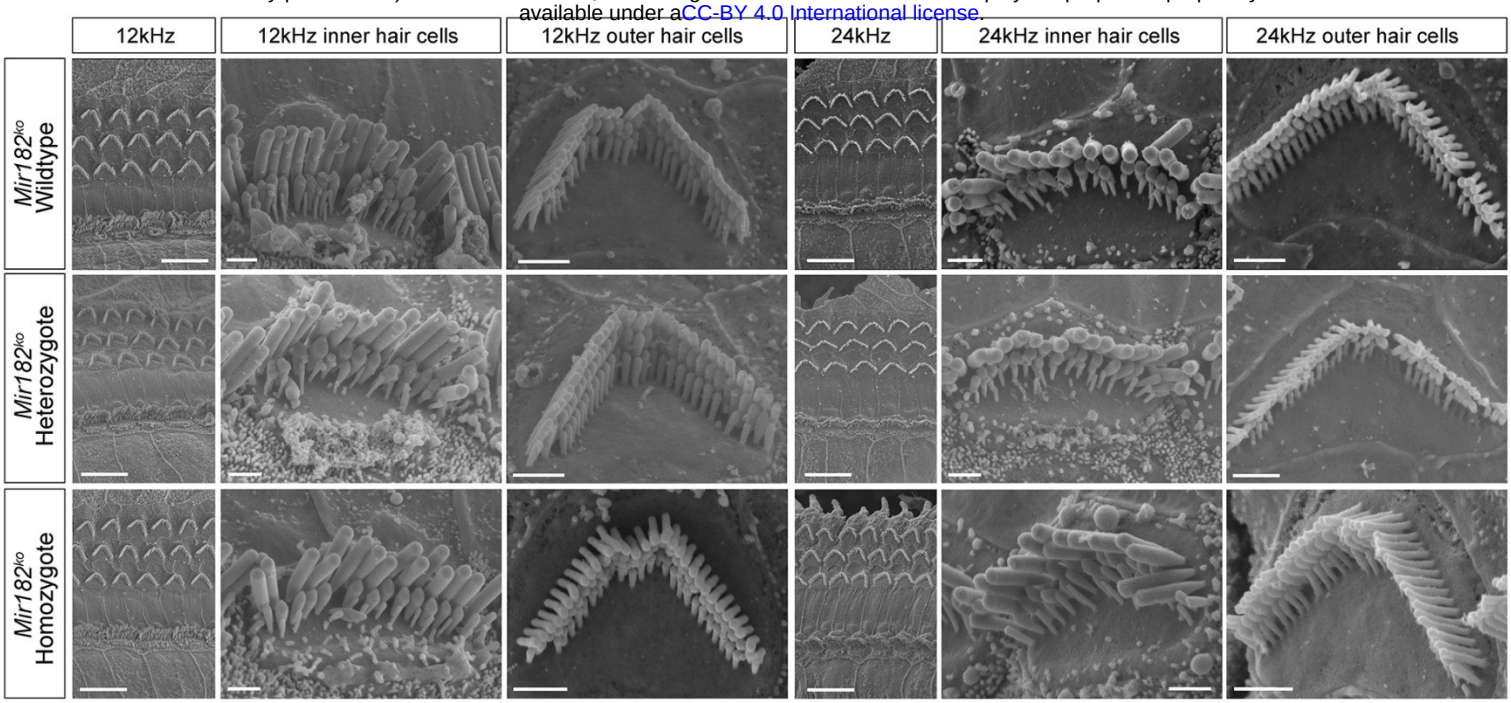

Figure 4. Scanning electron micrographs of *Mir182*^{ko} mice at P56. Two best-frequency regions of the organ of Corti are shown; 12kHz (68% of the way along the organ of Corti from base to apex) and 24kHz (43% of the way along the organ of Corti from base to apex). For each region, the left-hand column shows a zoomed-out image with inner and outer hair cell rows (scale bars=10µm), and the other two columns show an inner and an outer hair cell close up (scale bars=1µm). The top row shows wildtype hair cells (n=1), the middle row shows heterozygote hair cells (n=2) and the bottom row shows homozygote hair cells (n=3).

bioRxiv preprint doi: https://doi.org/10.1101/579003; this version posted March 16, 2019. The copyright holder for this preprint (which was not certified by peer review) is the author/funder, who has granted bioRxiv a license to display the preprint in perpetuity. It is made available under aCC-BY 4.0 International license.

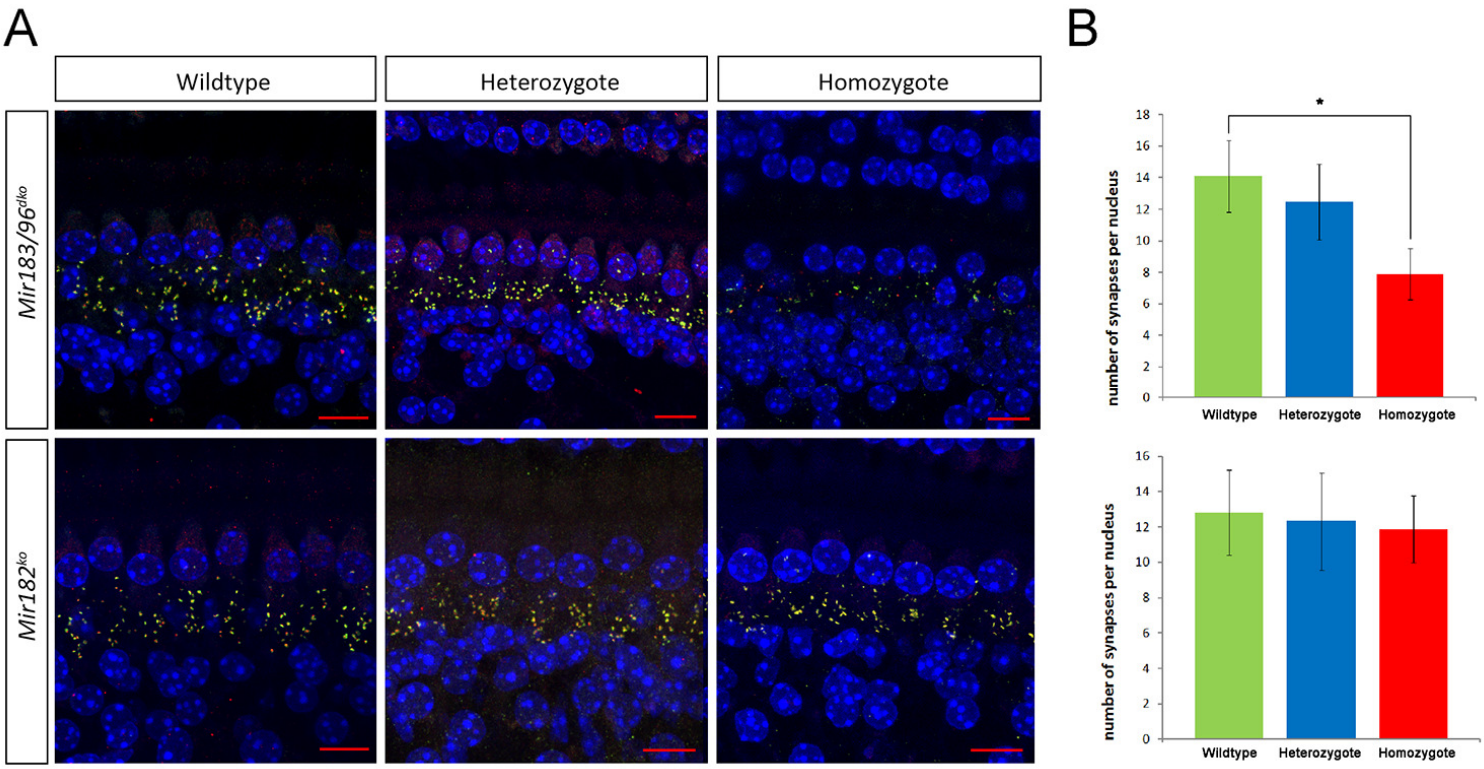

Figure 5. Colocalised pre- and postsynaptic densities in *Mir183/96*^{dko} and *Mir182*^{ko} mice.

A. Labelled synapses in *Mir183/96*^{dko} (top) and *Mir182*^{ko} (bottom) wildtype (left), heterozygous (middle) and homozygous (right) knockout mice. Presynaptic ribbons are labelled with anti-Ribeye antibody (red) and postsynaptic densities with anti-GluR2 antibody (green); where they colocalise, the resulting colour is yellow. Scale bar = 10µm.

B. Mean counts of colocalised pre- and postsynaptic markers in wildtype (green), heterozygous (blue) and homozygous (red) *Mir183/96*^{dko} (top) and *Mir182*^{ko} (bottom) mice. There are significantly fewer colocalised synapses in *Mir183/96*^{dko} homozygotes (n=3) compared to wildtypes (n=5, *p = 0.036, Wilcoxon rank sum test) but no significant differences in heterozygotes compared to wildtypes (n=7, p=0.76, Wilcoxon rank sum test). Synapse counts in *Mir182*^{ko} knockout heterozygotes (n=6) and homozygotes (n=7) showed no significant difference from wildtype (n=4, p=1.0, p=0.79 respectively, Wilcoxon rank sum test). Error bars show standard deviation.

bioRxiv preprint doi: https://doi.org/10.1101/579003; this version posted March 16, 2019. The copyright holder for this preprint (which was not certified by peer review) is the author/funder, who has granted bioRxiv a license to display the preprint in perpetuity. It is made available under aCC-BY 4.0 International license.

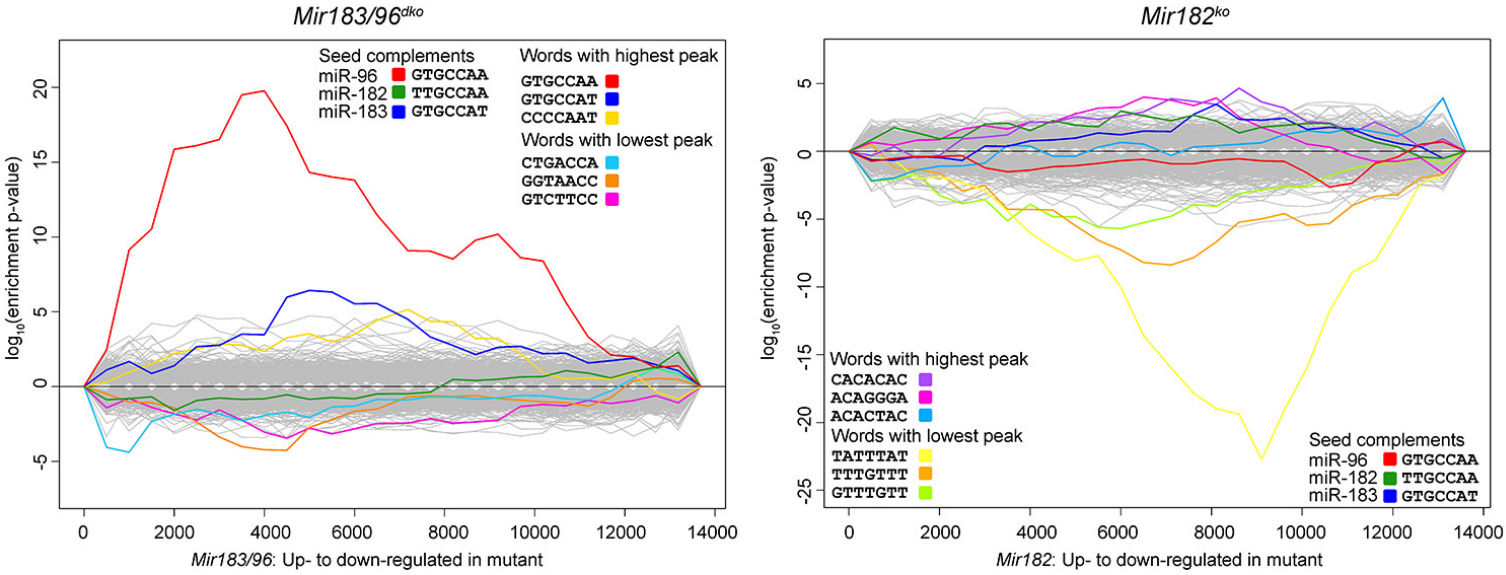

Figure 6. Sylamer analysis showing enrichment and depletion of heptamers in 3'UTRs in *Mir183/96*^{dko} homozygous mice (left) and *Mir182*^{ko} homozygous mice (right). The x-axis represents the sorted gene list from most up-regulated on the left to most down-regulated on the right. The y-axis shows the hypergeometric significance for enrichment or depletion of heptamers in 3'UTRs. UTRs are considered in bins, starting with the 500 most up-regulated genes on the left and increasing cumulatively until all genes have been considered. Lines indicate the enrichment of each heptamer; positive values indicate enrichment and negative values indicate depletion. The three words with the highest peaks and the three with the lowest peaks are highlighted in colour, as are the three heptamers complementary to the seed regions of miR-96, miR-182 and miR-183. The yellow line in the *Mir182*^{ko} plot on the right, enriched in the downregulated genes of *Mir182*^{ko} homozygotes, resembles a portion of an AU-rich element. This may reflect a change in protein binding to 3'UTRs in the absence of miR-182 (see Results for details).

bioRxiv preprint doi: https://doi.org/10.1101/579003; this version posted March 16, 2019. The copyright holder for this preprint (which was not certified by peer review) is the author/funder, who has granted bioRxiv a license to display the preprint in perpetuity. It is made available under aCC-BY 4.0 International license.

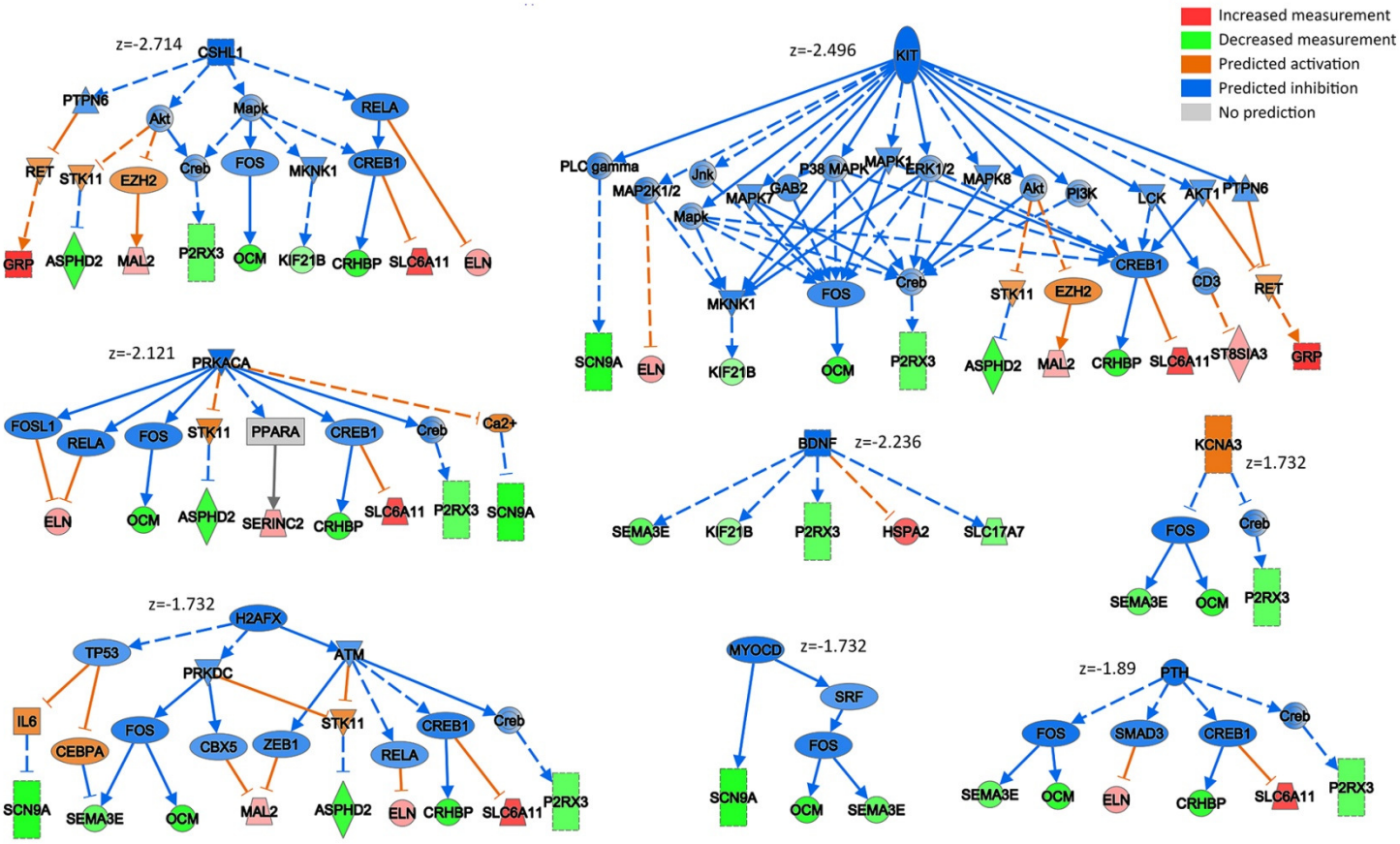

Figure 7. Networks generated by Ingenuity Pathway Analysis from the *Mir183/96*^{dko} RNA-seq data, showing predicted upstream regulators which may be responsible for some of the misregulation observed in the data. Misregulated genes are arranged on the lowest row, coloured according to observed misregulation (pink/red = upregulated, green = downregulated in mutants). The top row(s) contain predicted regulators (orange = predicted upregulation, blue = predicted downregulation). Predicted links inconsistent with the observed misregulation have been removed. The intensity of the colour indicates the level of observed or predicted misregulation. Dotted lines represent indirect regulation, and solid lines direct regulation. The z-score of each network, which is both a prediction of the direction of misregulation of the root regulator and a measure of the match of observed and predicted gene misregulation, is shown in the figure. A significant z-score is one with an absolute value greater than 2. A negative score indicates downregulation and a positive score upregulation of the root regulator.

bioRxiv preprint doi: https://doi.org/10.1101/579003; this version posted March 16, 2019. The copyright holder for this preprint (which was not certified by peer review) is the author/funder, who has granted bioRxiv a license to display the preprint in perpetuity. It is made available under aCC-BY 4.0 International license.

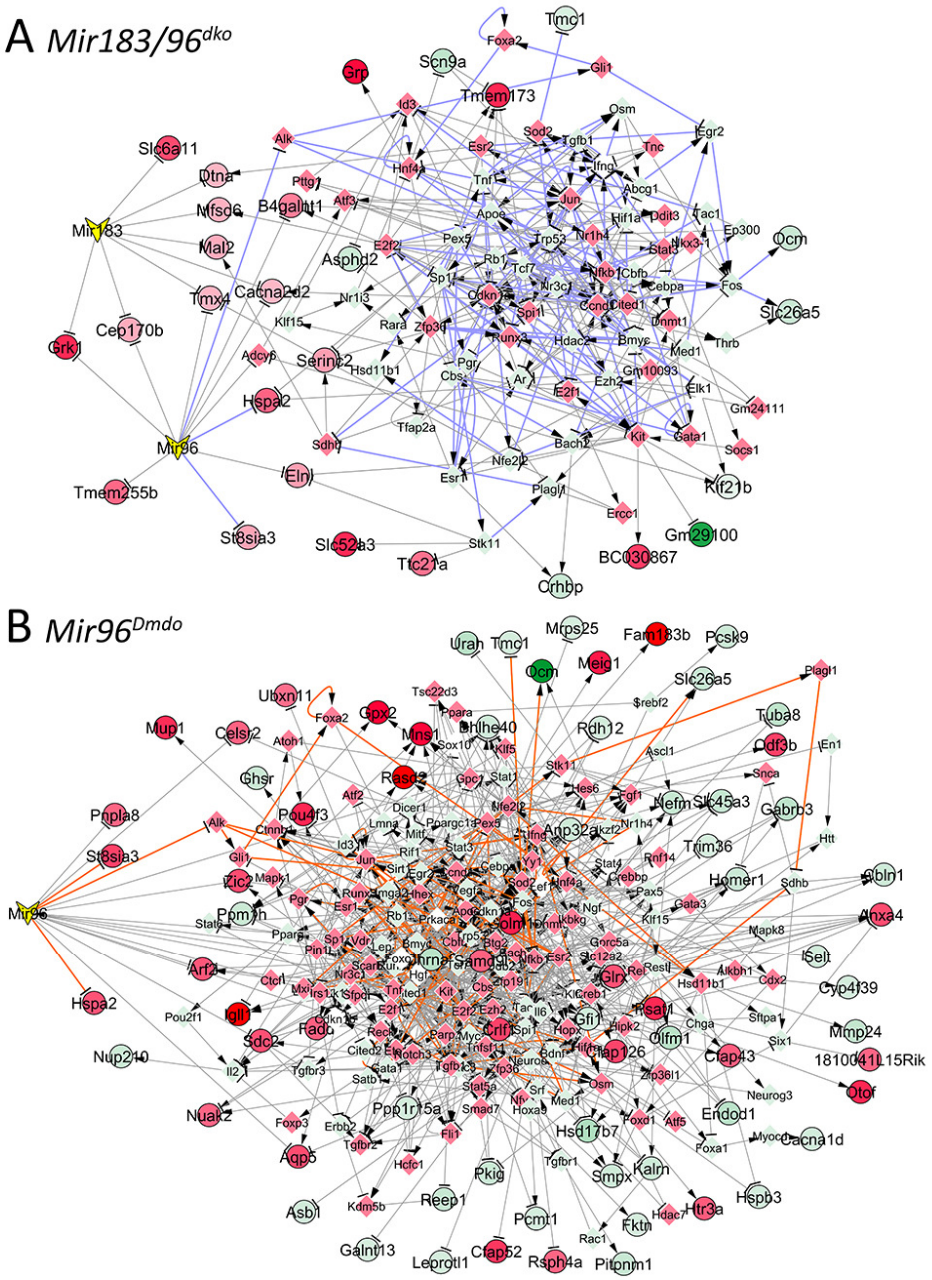

bioRxiv preprint doi: https://doi.org/10.1101/579003; this version posted March 16, 2019. The copyright holder for this preprint (which was not certified by peer review) is the author/funder, who has granted bioRxiv a license to display the preprint in perpetuity. It is made available under aCC-BY 4.0 International license.

Figure 8. A-D. Networks drawn using the PoPCoRN tool, based on the *Mir183/96*^{dko}, *Mir96*^{Dmdo} and *Mir182*^{ko} transcriptome data. The third network (C) shows the result of running the script with just the six genes found to be misregulated in both *Mir183/96*^{dko} and *Mir96*^{Dmdo} homozygotes (*Myo3a* could not be linked in to this network due to having no known regulators). Red indicates upregulation and green downregulation; circles with black borders show known misregulation in the organ of Corti and diamonds without borders show predicted misregulation. Violet lines in the *Mir183/96*^{dko} network (A) indicate edges also found in the *Mir96*^{Dmdo} network, and orange lines in the *Mir96*^{Dmdo} network (B) indicate edges also found in the *Mir183/96*^{dko} network.

bioRxiv preprint doi: https://doi.org/10.1101/579003; this version posted March 16, 2019. The copyright holder for this preprint (which was not certified by peer review) is the author/funder, who has granted bioRxiv a license to display the preprint in perpetuity. It is made available under aCC-BY 4.0 International license.

Expanded View legends

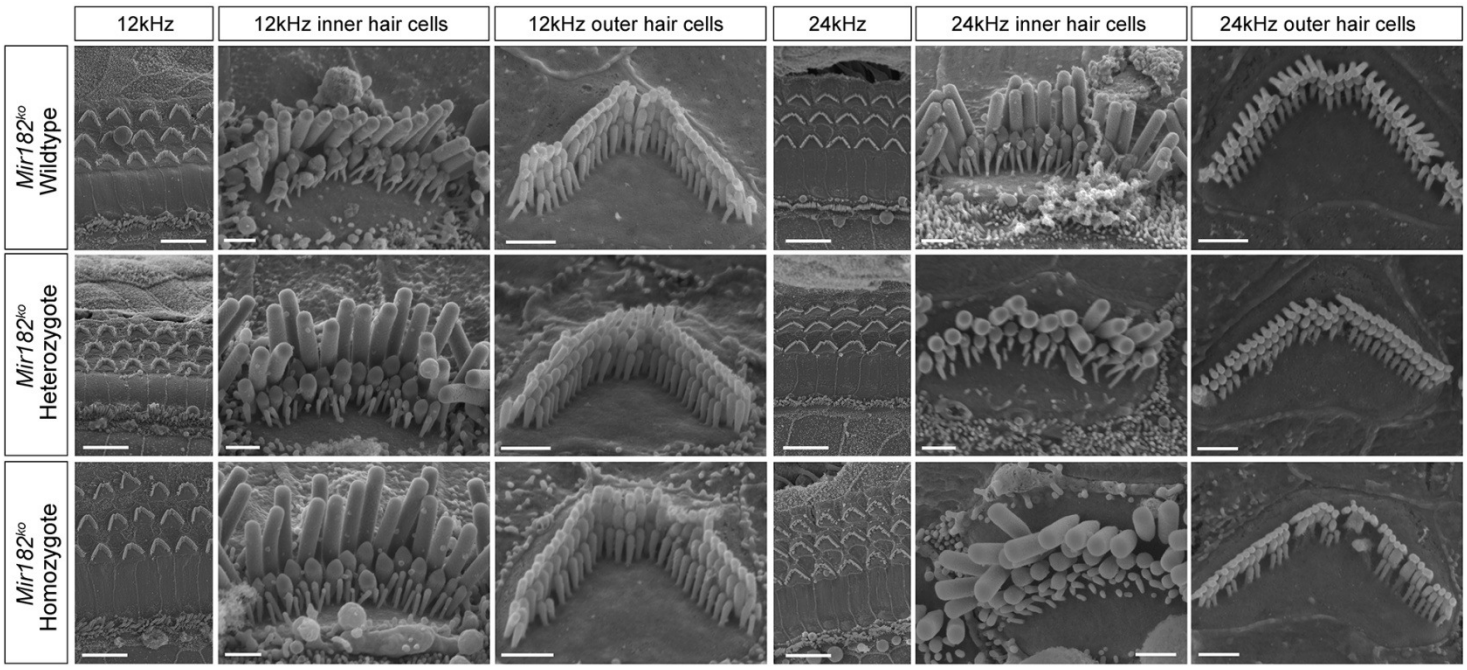

Figure EV1. Scanning electron micrographs of *Mir182*^{ko} mice at P28. Two frequency regions of the organ of Corti are shown; 12kHz (68% of the way along the organ of Corti from base to apex) and 24kHz (43% of the way along the organ of Corti from base to apex). For each region, the left-hand column shows a zoomed-out image with inner and outer hair cell rows (scale bars=10µm), and the other two columns show an inner and an outer hair cell close up (scale bars=1µm). The top row shows wildtype hair cells (n=1), the middle row shows heterozygote hair cells (n=2) and the bottom row shows homozygote hair cells (n=1).

bioRxiv preprint doi: https://doi.org/10.1101/579003; this version posted March 16, 2019. The copyright holder for this preprint (which was not certified by peer review) is the author/funder, who has granted bioRxiv a license to display the preprint in perpetuity. It is made available under aCC-BY 4.0 International license.

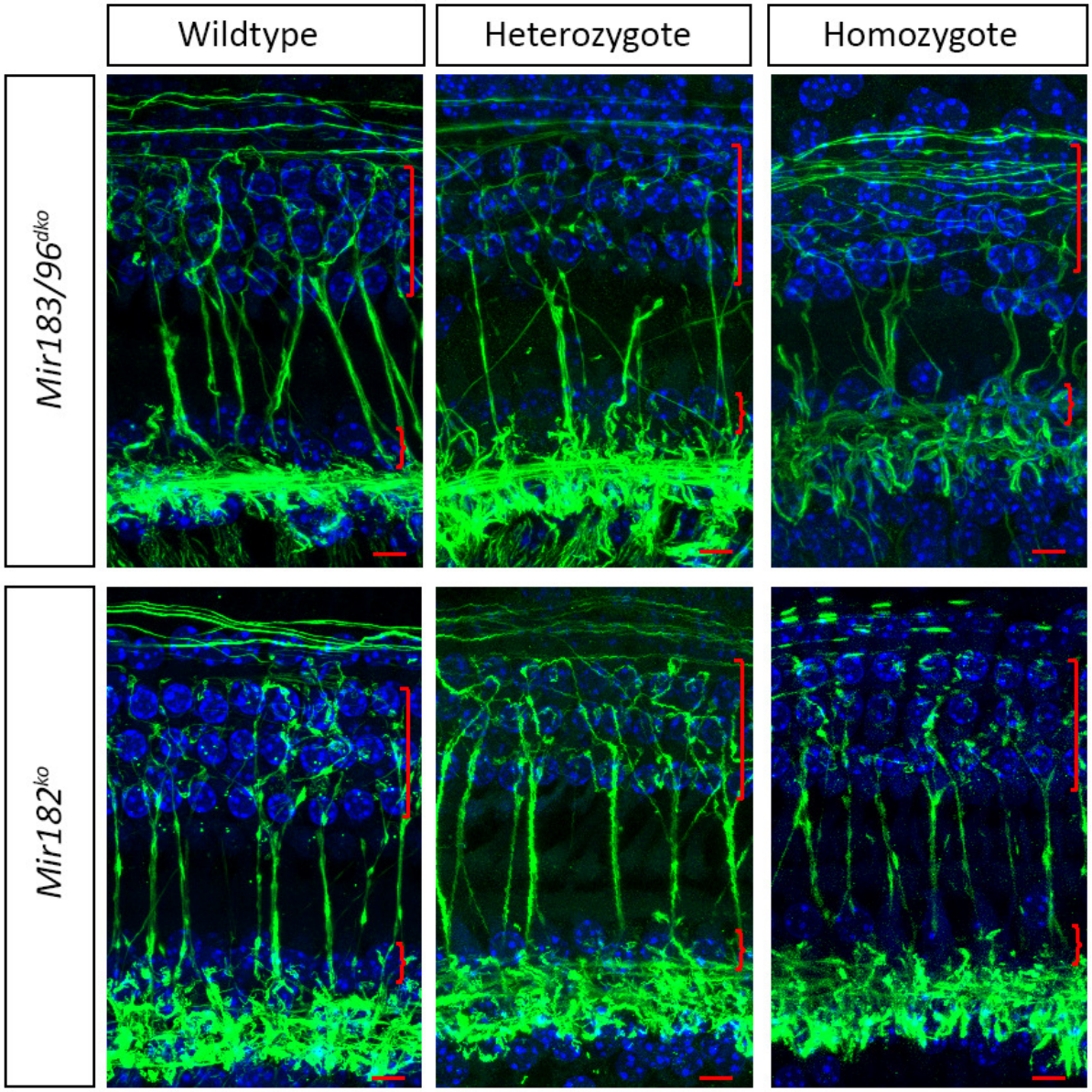

Fig EV2. Innervation of inner and outer hair cells of *Mir183/96*^{dko} mice (wildtype n=9, heterozygote n=8, homozygote n=4), and *Mir182*^{ko} mice (wildtype n=5, heterozygote n=6, homozygote n=10) at P28. Nerve fibres are stained with anti-neurofilament antibody (green) and nuclei are labelled with DAPI (blue). All panels show the 12kHz region. Square brackets indicate the three rows of outer hair cell nuclei, and curly brackets the single row of inner hair cell nuclei. Scale bar = 5µm.

bioRxiv preprint doi: https://doi.org/10.1101/579003; this version posted March 16, 2019. The copyright holder for this preprint (which was not certified by peer review) is the author/funder, who has granted bioRxiv a license to display the preprint in perpetuity. It is made available under aCC-BY 4.0 International license.

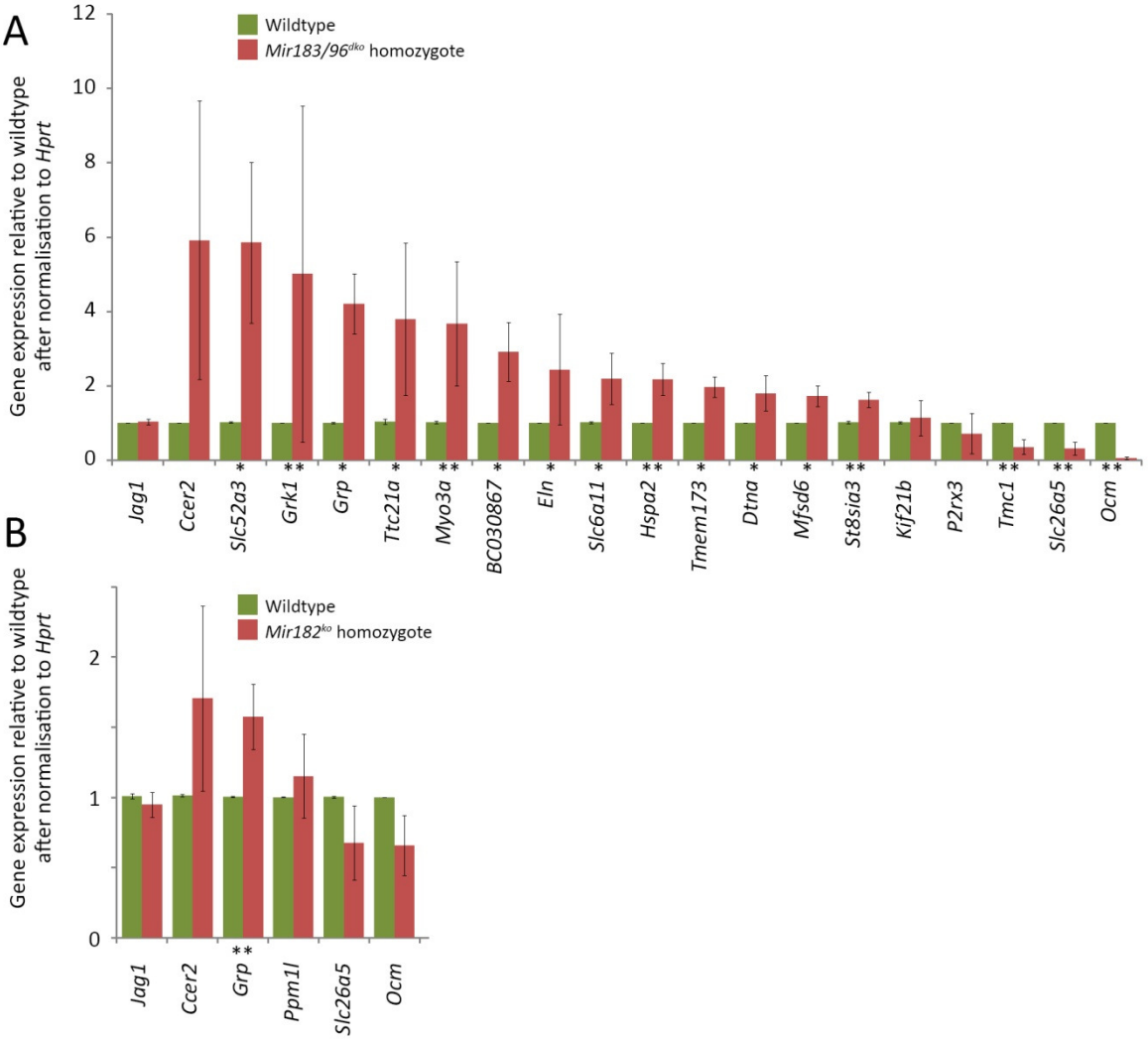

Fig EV3. Confirmation of RNA-seq results.

A, B. Testing gene expression in *Mir183/96*^{dko} (A) and *Mir182*^{ko} (B) homozygotes. qRTPCR was carried out on cDNA from P4 organs of Corti in wildtype (green; left bar) and homozygote (red; right bar) littermates to test gene expression changes. Six wildtype-homozygote pairs were tested for all genes except for *Ocm* and *Slc26a5* (6 wildtypes and 7 littermate homozygotes).

Data information: Error bars are standard deviation (* = P < 0.05, ** = P < 0.01). All p-values were calculated using the Wilcoxon rank sum test: A. *Jag1* p=0.38; *Ccer2* p=0.065; *Slc52a3* p=0.0022; *Grk1* p=0.0022; *Grp* p= 0.0022; *Myo3a* p=0.0022; *Ttc21a* p=0.065; *BC030867* p=0.0022; *Slc6a11* p=0.0022; *Eln* p=0.0022; *Hspa2* p=0.0022; *Tmem173* p=0.0022; *Mfsd6* p=0.0022; *Dtna* p=0.0022; *St8sia3* p=0.015; *Kif21b* p=0.39; *P2rx3* p=0.065; *Tmc1* p=0.0022; *Slc26a5* p=0.0012; *Ocm* p=0.0012. B. *Jag1* p=0.70; *Ccer2* p=0.065; *Grp* p=0.0022; *Ppm1l* p=0.39; *Slc26a5* p=0.065; *Ocm* p=0.065.

bioRxiv preprint doi: https://doi.org/10.1101/579003; this version posted March 16, 2019. The copyright holder for this preprint (which was not certified by peer review) is the author/funder, who has granted bioRxiv a license to display the preprint in perpetuity. It is made available under aCC-BY 4.0 International license.

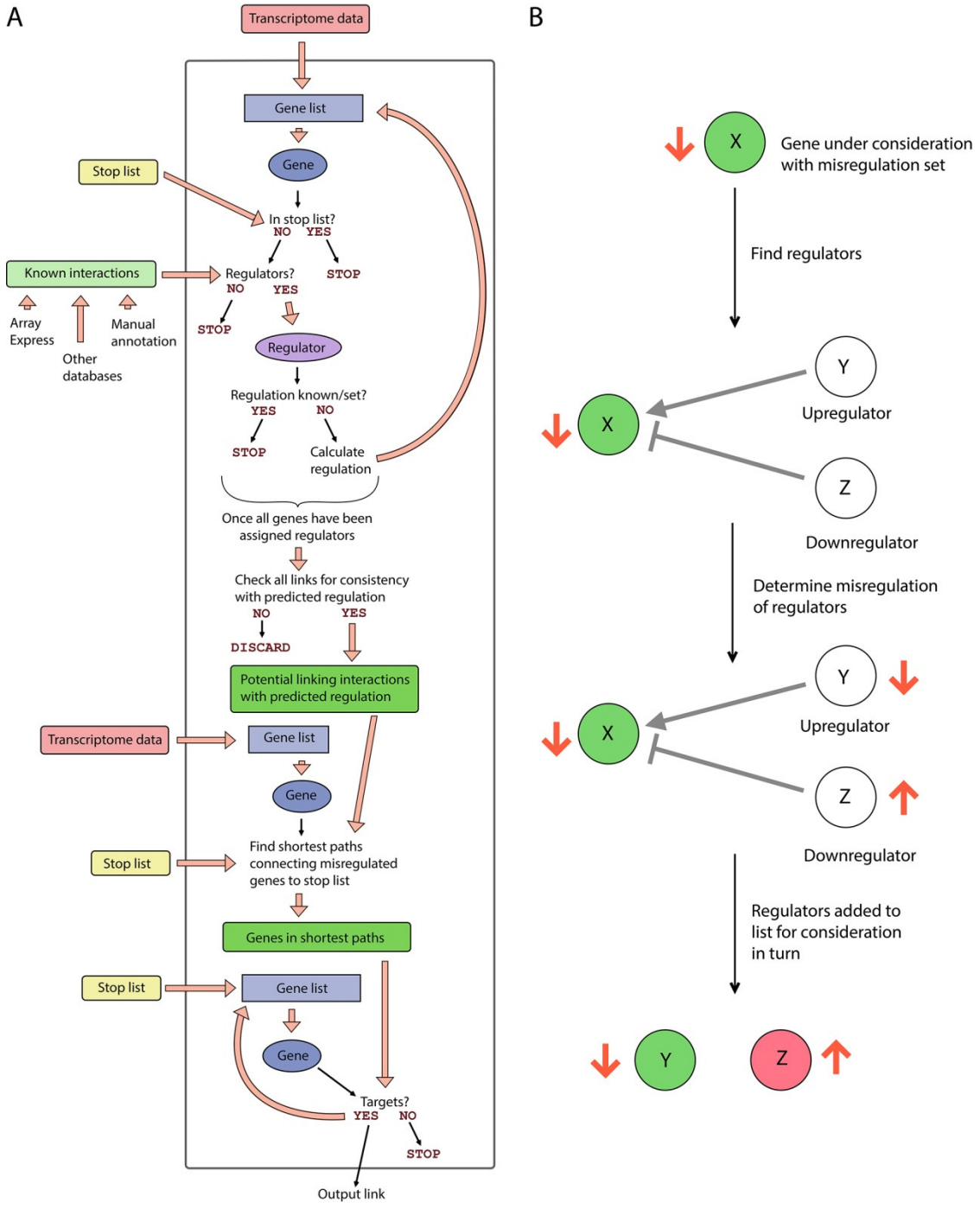

Fig EV4. The PoPCoRN script.

A. Schematic showing the steps of network construction carried out by the PoPCoRN script. The stop list is a list of genes at which the algorithm stops its upstream searching. In this case, the stop list consisted of the relevant microRNAs (*Mir182* for the *Mir182*^{ko}, and *Mir183* and *Mir96* for the *Mir183/96*^{dko}).

B. Diagram of the determination of direction of regulation of upstream regulators. Red arrows indicate direction of misregulation. Green indicates a downregulated gene, and pink an upregulated gene.

Mir183/96^{dko}				Seed matches			Confirmed by qPCR	Misregulation (logFC) in *Mir96*^{Dmdo}	
ID	logFC	FDR	Name	miR-96	miR-182	miR-183		P4	P0
ENSMUSG00000024517	1.894506	2.80E-09	Grp				yes		
ENSMUSG00000031450	1.662062	8.27E-09	Grk1	1	1	1	yes		
ENSMUSG00000059970	1.219381	6.89E-08	Hspa2	1			yes		0.427
ENSMUSG00000024349	1.672683	9.51E-07	Tmem173		1		yes		
ENSMUSG00000038457	1.174879	2.17E-06	Tmem255b	1					
ENSMUSG00000021680	-1.45986	1.16E-05	Crhbp						
ENSMUSG00000096641	2.329614	1.66E-05	Gm904						
ENSMUSG00000027463	1.661604	7.66E-05	Slc52a3				yes		
ENSMUSG00000029618	-1.48003	0.000288	Ocm				yes	-3.99	
ENSMUSG00000023232	0.752432	0.000574	Serinc2						
ENSMUSG00000075316	-1.71685	0.000624	Scn9a	1	1				
ENSMUSG00000041642	-0.72761	0.001914	Kif21b				no change in expression		
ENSMUSG00000025716	1.009586	0.001914	Myo3a				yes	0.402	
ENSMUSG00000070570	-0.9565	0.00233	Slc17a7						
ENSMUSG00000029015	-1.46283	0.004064	Slc26a5				yes	-0.606	
ENSMUSG00000072825	0.648798	0.004064	Cep170b	3	2	1			
ENSMUSG00000024749	-1.0624	0.008626	Tmc1		1		yes		
ENSMUSG00000006731	1.002458	0.012386	B4galnt1	2	1				
ENSMUSG00000099021	-2.80869	0.012386	Rn7s1						
ENSMUSG00000096257	2.270633	0.012386	Ccer2				not significantly upregulated		
ENSMUSG00000024479	0.650542	0.018223	Mal2			4			
ENSMUSG00000034773	1.502977	0.024181	BC030867				yes		
ENSMUSG00000041439	0.604453	0.026364	Mfsd6			1	yes		
ENSMUSG00000029675	0.75365	0.026364	Eln	2	2		yes		
ENSMUSG00000027071	-1.14813	0.026954	P2rx3			1	no change in expression		
ENSMUSG00000056812	0.713976	0.031747	St8sia3	2	1		yes	0.564	

bioRxiv preprint doi: https://doi.org/10.1101/579003; this version posted March 16, 2019. The copyright holder for this preprint (which was not certified by peer review) is the author/funder, who has granted bioRxiv a license to display the preprint in perpetuity. It is made available under aCC-BY 4.0 International license.

ENSMUSG00000100980	-6.1724	0.038628	Gm29100					
ENSMUSG00000029348	-1.40112	0.039429	Asphd2					
ENSMUSG00000010066	0.547453	0.04107	Cacna2d2	2	2	2		
ENSMUSG00000034723	0.58183	0.041107	Tmx4	1		1		
ENSMUSG00000032514	1.107432	0.043407	Ttc21a				yes	
ENSMUSG00000030307	1.408441	0.043407	Slc6a11			1	yes	
ENSMUSG00000024302	0.565905	0.046147	Dtna		1	1	yes	
ENSMUSG00000063531	-1.14147	0.048018	Sema3e			2		-0.138
Mir182^{ko}				**Seed matches**				
ID	**logFC**	**FDR**	**Name**	**miR-96**	**miR-182**	**miR-183**		
ENSMUSG00000027784	0.503152	0.000459	Ppm1l	2	3		no	
ENSMUSG00000024517	0.891914	0.007581	Grp				yes	
ENSMUSG00000096257	0.501143	0.03505	Ccer2				no	

Table EV1. Genes with a false discovery rate (FDR) < 0.05 are shown for *Mir183/96^{dko}* RNA-seq (top) and *Mir182^{ko}* RNA-seq (bottom). Green shading indicates downregulated genes, and pink upregulated genes. The presence of sequence complementary to the three microRNA seed regions in the 3'UTR of each gene is shown, as is the significant misregulation in *Mir96^{Dmdo}* mice at either P4 or P0.

bioRxiv preprint doi: https://doi.org/10.1101/579003; this version posted March 16, 2019. The copyright holder for this preprint (which was not certified by peer review) is the author/funder, who has granted bioRxiv a license to display the preprint in perpetuity. It is made available under aCC-BY 4.0 International license.